福　井　大　学　審　査
学 位 論 文 [博 士 (工 学)]

Diffusion-Controlled Current of Lithium Intercalation into Graphite

(グラファイト中へのリチウムのインターカレーション
の拡散電流)

平成十九年九月

王　暁　霞

University of Fukui

Fukui, Japan

A Dissertation Submitted to the University of Fukui for the

Doctor Degree of Engineering

Diffusion-Controlled Current of Lithium Intercalation into Graphite

(グラファイト中へのリチウムのインターカレーションの拡散電流)

by

Xiaoxia Wang

Board of Examiners (審査委員会)

Chairman:

Prof. Dr. Koichi Aoki (青木　幸一)

Examiners:

Prof. Dr. Jingyuan Chen (陳　競鳶)

Prof. Dr. Nobu kuzuu (葛生　伸)

Prof. Dr.Takashi Ogihara (荻原　隆)

September 2007

Table of contents

Abstract

Actually the commercial lithium-ion batteries unavoidably suffered from problems such as the safety problem, the efficiency decrease during the charge/discharge cycle and the aging. Efforts have focused on developing new materials such as carbonaceous anode and metal oxide cathode materials and the electrolyte solvents and salts compatible with them from a practical side. It is important and necessary to investigate the mechanism of these problems from the theoretical view point. However the fundamental understanding on the intercalation mechanism of lithium ion on carbon material electrodes (e.g. graphite) is relatively few. This thesis aimed at exploring and interpreting the kinetic process of lithium intercalation on graphite electrodes. It will be helpful to figure out the reason of charge loss and to improve the efficiency of lithium batteries.

The lithium intercalation into graphite has been known in the form of $Li^+ + C_6 + e^- \rightarrow LiC_6$. The intercalation process thus should be composed of the diffusion of lithium ion from solution to the graphite surface, the reduction of lithium ion occurring on the interface and the intercalation of reduced lithium atom from interface to the solid graphite. The process of the diffusion of lithium ion in solution involved the charge transfer (part (1)), and the current was verified to be diffusion-controlled. The transfer of reduced lithium atom from interface to the solid graphite was coupled with the mass transfer (part (2)) that is also controlled by diffusion. This work focuses on experimental and theoretical investigation on the above aspects electrochemically via. cyclic voltammetry, chronoamperometry, chronocoulometry, and spectroscopically via Raman spectroscopy.

(1): Charge transfer of Li^+ ion on pyrolytic graphite electrode in solution. Peak currents and potentials of voltammograms of lithium ion at the pyrolytic graphite electrode were obtained under the conventionally voltammetric conditions except for addition of supporting electrolyte. They were interpreted on the basis of the voltammetric concept in order to estimate rate-determining steps and redox potentials at zero current. The cathodic wave at concentrations less than 10 mM was controlled by diffusion and migration of lithium ion in the solution, whereas that at higher concentrations was by the intercalation kinetics. The anodic wave was caused by the de-intercalation, and behaved like an adsorption wave. The cathodic charge evaluated from the integration of the voltammogram was larger by 30% than the anodic one because of side reaction of acetonitrile or impurities. The anodic and the cathodic peak potentials extrapolated to zero current were, respectively, -1.58 and -2.11 V vs. Ag|AgCl, which can be regarded as universal

values. The crystallinity of graphite electrode was investigated by Raman spectroscopy. The difference in the peak potentials of intercalation and de-intercalation is 0.53 V, equivalent to 51 KJ mol^{-1}. This energy is an interfacial kinetic contribution of the intercalation and/or de-intercalation, and hence is lost at a cycle of the charge/discharge. A technique of reducing this voltage should be an important subject to improving energetic efficiency of lithium batteries.

(2): Mass transfer of Li inside the solid graphite. Intercalation current of Li^+ to a graphite electrode varied sharply with $[Li^+]$ from the proportionality to a constant, exhibiting critical behavior at $[Li^+]$ =10 mM. The voltammetrically cathodic peak current, which is caused by the intercalation, was proportional to the square-root of the scan rate, irrespective of the concentrations. The current for $[Li^+]$ < 10 mM is controlled both by diffusion and electric migration of Li^+ in solution, whereas that for $[Li^+]$ > 10 mM is controlled by diffusion of Li in the graphite. In order to validate the critical behavior, the time-dependent mass transport theory was developed by use of the Nernst-Planck equation for the solution phase and the diffusion equation for the graphite one. Both equations were combined at the interface through a kind of the Nernst equation which contained a maximum concentration of Li in the graphite predicted from the structure of LiC_6. The theory supported the critical behavior in the potential domain of the limiting current. From the critical concentration, the diffusion coefficient of Li in the graphite was estimated to be 0.79×10^{-11} cm^2 s^{-1}, independent of the concentrations. The time-dependent mass transport theory proposed here can be used as referenced method to the investigation of lithium intercalation into other synthesized materials and to evaluate the diffusion coefficient of lithium intercalation.

Chapter 1

Overview of lithium batteries

1.1 The history and state of lithium batteries

Lithium has long been paid much attention as a promising anode material of batteries. It has two unique properties: (1) the highest standard reduction potentials (-3.0 V vs SHE), and (2) and the lightest metal (0.534 g cm^{-3}) [1]. The combination of these two characteristics gives the element a particularly favourable energy content, with a theoretical specific capacity of 3860 Ah kg^{-1} in comparison with 820 Ah kg^{-1} for zinc and 260 Ah kg^{-1} for lead. In that the standard reduction potential of lithium [2] is more negative than -3.0 V it can be translated into high cell voltage when it is combined with a given cathode. The development of lithium batteries comes from non-rechargeable primary lithium battery to rechargeable lithium ion battery.

The pioneer work with the lithium battery began in 1912 under G.N. Lewis. In the 1950s lithium metal was found to be stable in a number of non-aqueous solvents despite its reactivity [3]. Intensified research activities resulted in the commercialization of the first non-rechargeable lithium batteries (primary lithium batteries) in the 1960s and 1970s. The continued efforts to expand lithium chemistry into rechargeable technology, however, encountered severe difficulties in terms of the cycle life and safety [4,5]. Soon it was realized that the source of the problems was the morphology of the lithium crystals newly deposited from the electrolytes upon recharge [6,7]. Dendrite of lithium crystals grows on the anode upon charge and, during the subsequent discharge, and becomes electrically isolated from the substrate due to non-uniform dissolution rates at different sites of the dendrite. The direct victim of such lithium loss is energy density, because excessive lithium has to be used in the cell to make up for the loss [8]. But more seriously, a hazard could be caused by such dendrite, which is electrochemically inactive but chemically hyper-reactive due to their high surface area. When dendrite growth pierces the separator and results in an internal short, thermal runaway and explosion ensue.

The failure of lithium as an anode due to dendrite formation prompted the search for a way to circumvent the drastic morphological change of the anode during cell cycling. As a result, “host-guest” chemistry was considered. Also known as “intercalation” or “insertion” type electrodes, this concept of reversible chemistry had been applied earlier to cathode materials for lithium batteries, as represented by the trailblazing work of Whittingham [9,10] and the significant

improvements by Goodenough et al. and others [11,12]. Most of the host materials are transition metal oxides or chalcogenides with stable crystal lattices, and their layer or tunnel structures provide the pathways for guest ions such as the lithium ion to diffuse. By injecting or extracting electrons, the redox reactions occur on the host lattice while mobile guest ions intercalate into or de-intercalate from the host matrix to compensate for regional electroneutrality. During the whole intercalation/de-intercalation cycle, there are no Faradaic changes in the "guest ion". If a similar intercalation host could be found and used as an anode material, then a battery employing such intercalation cathodes and anodes would only require the lithium ion to shuttle back and forth between the electrodes without the presence of lithium metal. The nickname "rocking-chair battery" was given to such a device that uses dual intercalation electrodes [13], the working principle of which is schematically depicted in Figure 1-1 [14]. During the charging process, Li ions move from the cathode material through the electrolyte into the carbon anode material. During discharge, the movement occurs in the reverse direction. The concept of rocking-chair lithium batteries was confirmed experimentally by using lithiated oxides ($Li_6Fe_2O_3$, $LiWO_2$) as interaction anodes and other oxides (WO_3, TiS_2, V_2O_5) as cathodes in non-aqueous electrolytes [15,16]. However, the enhanced safety and extended cycle life were not sufficient to offset the penalty in energy density caused by the replacement of lithium metal; hence, these systems were never commercialized [17,18]. A breakthrough was made when Japanese researchers exploited an old concept of using carbonaceous materials as anode intercalation host [19-21]. The term "lithium ion battery" that was introduced by those researchers eventually prevailed and replaced the other aliases such as "rocking-chair" [13], "shuttlecock" [22], or "swing" batteries [23]. In the charged state of these carbonaceous anodes, lithium exists in its ionic rather than metallic state, thus eliminating any possibility of dendrite lithium. The advantage of this new host is highlighted by the low cost of carbon and the high lithium ion

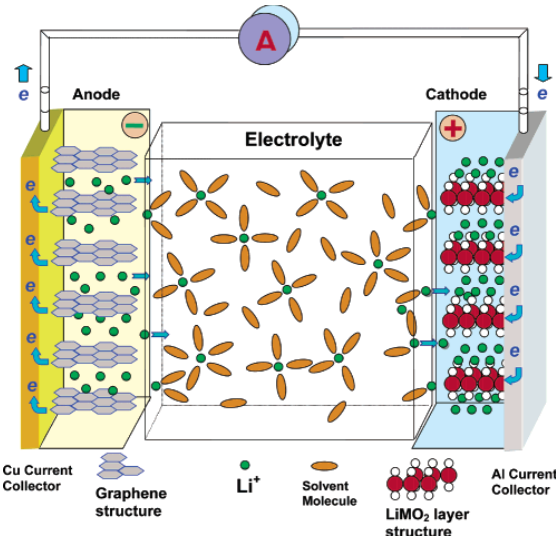

Fig 1-1. Schematic description of a "(lithium ion) rocking-chair" cell that employs graphitic carbon as anode and transition metal oxide as cathode. The undergoing electrochemical process is lithium ion deintercalation from the graphene structure of the anode and simultaneous intercalation into the layered structure of the metal oxide cathode. For the cell, this process is discharge, since the reaction is spontaneous.

activity in the intercalation compound; the latter renders an anode potential close to that of lithium metal and minimizes the energetic penalty. In 1990 Sony [24] announced the commercialization of lithium-ion batteries based on petroleum coke and $LiCoO_2$. In the same year Dahn and co-workers published their seminar report on the principle of lithium intercalation chemistry with graphitic anodes and the effect of electrolyte solvent in the process [25]. The decade following Dahn's publication caused an explosive growth in lithium ion technology research, while the main excitement revolved around developing new materials such as carbonaceous anode and metal oxide cathode materials and the electrolyte solvents and salts compatible with them. The result of those intensified efforts was the successful commercialization and the rapid thriving of this youngest battery chemistry. The employment of new materials and novel engineering designs has pushed the cycle life, energy, and power density of this technology to more than 2000 cycles, 160 Wh kg^{-1}, and 5000 W kg^{-1}, respectively [26]. The major driving force of this market remains the so-called "small formula batteries" with capacities smaller than 1 Ah; however, industry-size lithium ion cells are increasingly being used in space, military, and other special applications, especially as traction power sources for electric or hybrid electric vehicle (EV/HEV) applications [26].

1.2 The electrolyte

Most compositions of lithium electrolytes are based on solutions of one or more lithium salts in mixtures of two or more solvents, and single-solvent formulations are very rare, if there are any. The rationale behind this mixed solvent formulation is that the diverse and often contradicting requirements of battery applications can hardly be met by any individual compound, for example, high fluidity versus high dielectric constant; therefore, solvents of very different physical and chemical natures are often used together to perform various functions simultaneously. In accordance with the basic requirements for electrolytes [14], an ideal electrolyte solvent should meet the following minimal criteria: 1)It should dissolve salts to sufficient concentration. In other words, it should have a high dielectric constant (ε). (2)It should be fluid (low viscosity η), so that facile ion transport can occur. (3)It should remain inert to all cell components, especially the charged surfaces of the cathode and the anode, during cell operation. (4) It should remain liquid in a wide temperature range. In other words, its melting point (Tm) should be low and its boiling point (Tb) high. (5) It should also be safe (high flash point Tf), nontoxic, and economical. The following section will introduce some electrolytes which were frequently used in lithium ion

batteries.

1.2.1 Propylene carbonate (PC)

Among various solvents, cyclic diesters of carbonic acid have undoubtedly attracted the main research attention throughout the entire history of lithium batteries. However, the early interest in these compounds arose solely from their high dielectric constant and, hence, their ability to dissolve a wide variety of lithium salts. In 1958, it was observed that lithium could be electrodeposited from a solution of $LiClO_4$ in PC [27], and PC became the immediate focus of investigation [3,4,5]. Its wide liquid range, high dielectric constant, and static stability with lithium made it a preferred solvent. But the poor cycling efficiency of lithium cells with PC electrolytes was soon recognized due to intrinsic property of PC and the reaction between PC and the newly deposited lithium particles [4]. More recent studies by spectroscopy have confirmed the PC reduction on a newly formed lithium surface [28].

1.2.2 Ethers

In view of the poor cycling efficiency and the potential hazards associated with PC, ethers have been focused for improved lithium morphology. In the 1980s, ethers were widely preferred by researchers as an alternative candidate, because of their low viscosity and resultant high ionic conductivity, but, most of all, the better lithium morphology during cycling [29]. The formation of dendritic lithium seemed to be sufficiently suppressed in these solvents even at high charge rates [30]. However, efforts to incorporate ether-based electrolytes in lithium cells were still troubled by the poor capacity retention [31-33], and prolonged cycling (>100 cycles) of the cells still produced dendrite deposition [34], which terminated the cells by creating shorts [35], despite the improved lithium morphology observed in the short term. In addition to the problem with the lithium anode, a new factor contributing to the capacity fade surfaced as the oxidative decomposition of ether-based compounds on the cathode surface [36-38]. During the 1990s, various ethers were gradually phased out in most of the electrolyte systems under investigation.

1.2.3 Ethylene carbonate (EC)

In the first generation of the commercial lithium ion cells, a PC-based electrolyte was used by Sony [24]. However, the real renaissance for using alkyl carbonates as lithium electrolyte solvents was not brought about by PC but, quite unexpectedly, by its high melting cousin EC. Compared with PC, EC has comparable viscosity and slightly higher dielectric constant, which are favorable merits for a solvent candidate. In fact, its dielectric constant is even higher than that of the most common electrolyte solvent on the earth: water (ε~79) [1]. However, because of its high

melting point (~36 °C), it was never favored as an ambient-temperature electrolyte solvent in the early days of lithium battery research: the liquid range of the electrolytes based on it would be too restricted. EC was considered as an electrolyte co-solvent for the first time by Elliot in 1964, who noted that, due to the high dielectric constant and low viscosity of EC, the addition of it to electrolyte solutions would favor ion conductivity [39]. Electrolytes based on EC as compared with PC demonstrated improvements, not only in bulk ion conductivity but also in interfacial properties such as lower polarization on various cathode surfaces [40]. Following these reports, EC began to appear as an electrolyte co-solvent in a number of new electrolyte systems under investigation, many of which still contained ethers [35,38,41-44]. However, the first commercialized rechargeable lithium battery used an ether-free composition, an EC/PC mixture, as the electrolyte solvent [45-46]. The unique position of EC as a lithium battery electrolyte was established in 1990 when Dahn and co-workers reported the fundamental difference between EC and PC in their effects on the reversibility of lithium ion intercalation/ de-intercalation with graphitic anodes [25].

1.2.4 Linear carbonates

After Sony successfully marketing the first generation lithium ion cells, with the energetic advantage of highly crystalline carbon (graphitic) over disordered carbon being recognized, EC became the core and indispensable component of the electrolyte formulation. During the early 1990s, efforts were made to expand the limited liquid range of EC-based electrolytes by using different co-solvents, including PC [47-48], THF and 2-Me-THF [38,41-44], diethoxyethane (DEE) [49-50], and dimethoxyethane (DME) [51-54]. In 1994 Tarascon and Guyomard used a linear carbonate, dimethyl carbonate (DMC), as a co-solvent with EC first and described it in open literature [55-56]. As it has been pointed out, linear carbonates differ from their cyclic cousins by their low boiling points, low viscosity, and low dielectric constant. They can form homogeneous mixtures with EC at any ratio, and the resultant mixed electrolytes benefit not only from the melting-temperature suppression of EC but also from the low viscosity (higher ion conductivity) of DMC. It seems that a synergistic effect is achieved when EC and DMC (or other linear carbonates) are mixed because the merits of each individual solvent are imparted on to the resultant mixture: high anodic stability of EC on cathode surfaces, high salvation power of EC toward lithium salts, and low viscosity of DMC to promote ion transport. This new formulation of electrolytes based on a mixture of EC with a linear carbonate was quickly adopted by the researchers and manufacturers [54,57-60]. Other linear carbonates were also explored, including

DEC [61-63], ethylmethyl carbonate (EMC) [64], and propylmethyl carbonate (PMC) [65-66].

1.3 Lithium salts

An ideal electrolyte solute for ambient rechargeable lithium batteries should meet the following minimal requirements: (1)It should completely dissolve and dissociate in the non-aqueous media, and the solvated ions (especially lithium cation) should move in the media with high mobility. (2)The anion should be stable against oxidative decomposition at the cathode. (3)The anion should be inert to electrolyte solvents. (4)Both the anion and the cation should remain inert toward the other cell components such as separator, electrode substrate, and cell packaging materials. (5)The anion should be nontoxic and remain stable against thermally induced reactions with electrolyte solvents and other cell components. The salts including lithium perchlorate ($LiClO_4$) and various lithium borates, arsenates, phosphates, and antimonates, $LiMX_n$ (where M=B or As, P, and Sb and n=4 or 6, respectively) were summarized below.

$LiClO_4$ has been a popular electrolyte solute owing to its satisfactory solubility and high conductivity (~9.0 mS cm^{-1} in EC/DMC at 20 °C) as well as its high anodic stability (up to 5.1V on a spinel cathode surface in EC/DMC) [56]. However, the high oxidation state of chlorine (VII) in perchlorate makes it a strong oxidant, which readily reacts with most organic species in violent ways under certain conditions. Actually, in the 1970s it had already been realized that $LiClO_4$ was impractical as an electrolyte solute for industry purposes [67]; nevertheless, it is still frequently used as a salt of convenience in various laboratory tests because it is easy to handle and economical [68,47].

$LiPF_6$ was the obvious winner and was eventually commercialized. The success of $LiPF_6$ was not achieved by any single outstanding property but, rather, by the combination of a series of well-balanced properties with concomitant compromises and restrictions. The $LiPF_6$ solution in mixed carbonates remains one of the most conducting salts and can effectively resist oxidation up to 5.1V [56], thus making it one of the few salts that can actually support the operation of 4.0V cathode materials.

$LiAsF_6$ was paid attention during the late 1970s. It was a superior salt to $LiClO_4$ as an electrolyte solute for lithium batteries [69]. For a long period, the combination of $LiAsF_6$ with various ethers became the most popular system under investigation [29,31,70].

$LiBF_4$ was out of favor in the early days of lithium battery research because it leads to poor lithium cycling efficiencies, which decayed rapidly with cycle number [29,71]. The use of

$LiBF_4$ in lithium-based cells has been rare because of its inferior ion conductivity until recently, when the thermal instability of $LiPF_6$ and the moisture sensitivity became recognized. Attempts to replace $LiPF_6$ in lithium ion cells have been made, and the cells based on $LiBF_4$ electrolytes showed improved performance, not only at elevated temperatures up to 50°C [72] but, surprisingly, also at low temperatures as well [73].

Lithium trifluoromethanesulfonate (LiTf) [74] belongs to another family of lithium salts. It is based on the conjugate bases of the organic superacids, where acid strength is increased because of the stabilization of anions by the strongly electron-withdrawing groups, usually perfluorinated alkyls. One major drawback of these sulfonate salts is their poor ion conductivity in non-aqueous solvents as compared with other salts. The real obstacle that eventually eliminated LiTf as a candidate for lithium ion battery application is the serious aluminum corrosion that occurred in LiTf based electrolytes.

Lithium bis(trifluoromethanesulfonyl)imide (LiIm) and its derivatives [51] sparked considerable hope that it might replace the poorly conducting LiTf, the hazardous $LiClO_4$, the thermally unstable $LiBF_4$ and $LiPF_6$, and the toxic $LiAsF_6$ in lithium battery applications [74]. Despite all of these merits, the application of LiIm in lithium ion cells never materialized because it caused severe Al corrosion in electrolytes based on it [75].

Beside the above often used lithium salts, now many new kinds of salts have been introduced to the field of lithium batteries such as lithium tris(trifluoromethanesulfonyl)methide (LiMe) [76], lithium borates with aromatic ligands [77], lithium borates with nonaromatic ligands [78], lithium chelatophosphates [79-80], lithium fluoroalkyl phosphates (LiFAP), and lithium salts based on heterocyclic anions [81].

1.4 Electrode materials

In a practical Li-ion battery, multiple layers of anodic and cathode materials are assembled together with appropriate separators. In typical cylindrical cells, the electrodes are bound as a roll with two separators, and the electrolyte fills the gap between the anode and cathode compartments.

1.4.1 Anode materials

The carbon anode material itself is prepared by dispersing the selected carbon materials along with a binder such as poly(vinylidene fluoride) (PVdF) on a current collector [82]. The carbon materials on the literatures may be classified into three groups. (1)The basic studies using

HOPG or natural graphite material throw light on many fundamental questions relating to graphite intercalation chemistry. (2)A number of modified graphite materials or composite materials are employed for practical applications. (3)There is still considerable interest in improving the hard carbon materials for battery applications.

1.4.1.1 Graphite materials

The intercalation/de-intercalation studies have been mainly carried out on natural graphite material and these studies are still in progress. Comprehensive reviews on many of these aspects are available [83-84]. The voltammograms [83] obtained on natural graphite electrode material clearly indicate the different potential regions which correspond to stage transitions on graphite electrodes. But because many limitations, only the edge plane fraction of the natural graphite flakes contribute to the intercalation/de-intercalation process. HOPG electrodes may indeed be considered as a better model of graphite material since the electrochemical process can be studied systematically on the basal plane or on the edge oriented plane by proper alignment of the working electrode. It is interesting to note that Basu [85] has employed HOPG as an anode material in one of the initial battery systems developed with LiC_6 [85]. The kinetics of electron transfer and diffusion of Li^+ into the HOPG matrix has been investigated using EIS [86].

1.4.1.2 Modified graphite materials

The main cause for the limited success of natural graphite material appears to be the large crystal size and the probability of higher irreversible surface damage. A variety of strategies have been adopted to modify graphite materials in order to overcome this difficulty. The most successful of these attempts appear to be the use of mesocarbon microbeads (MCMB) and graphite fibres. There are four common forms of carbon particles namely MCMB, fibres, fakes and potatoes. The average particle-size of these materials is in the 2 mm range.

Detailed procedures for the preparation of MCMB and their characterisation are well documented [87]. MCMB shows low level of irreversible capacity [88]. Among graphitic materials, low crystallinity and minimum surface-area due to the spherical nature of the particles appear to be the advantageous features of MCMB [89].

Fibres are the second type of materials that have proved to be successful negative electrodes in Li-on batteries. They are either prepared from pitch-based slurries or vapour grown as carbon fibres. The optimization studies have been reported for vapour grown carbon fibre (VGCF) [90].

Apart from the two types of graphite materials mentioned above, different

graphite-powders have been evaluated for potential application as host lattices for intercalation of lithium ions. The particle-size, the porosity and packing density of graphite particles [91] show considerable influence on intercalation/deintercalation efficiency of powdered coke. Graphite particles obtained from heat-treated gas cokes show lithium-ion interactions which depend on grain size and over all BET surface-area [92]. Different types of milling operations appear to influence the electrode performance differently [93].

A wide variety of additives, which range from non-graphitic carbon materials to polymers, gels, host materials and metals, have been added to natural as well as synthetic graphite to improve electrode performance. Forming a thin layer of acetylene black and natural graphite on graphite fibres [94], coating coke on synthetic graphite [95], coating the graphite particles with polymeric materials [92], incorporating siloxanes [96] and silicon [97] on graphite surface reduce the irreversible capacity and increases the cycle efficiency. Boron-doped [98] graphite materials improve the crystallinity of graphite considerably. Inclusion of tin and SnO or some metal such as bismuth, gold, palladium, zinc, silver and tin increased both the reversible and the irreversible capacities [99-100]. Incorporation of copper and nickel was found to be effective in improving the cycle-life of graphite materials.

1.4.1.3 Non-graphitic carbons

Compared with the graphitization of carbon, Non-graphitic carbon materials require much lower heat treatment temperature and, hence, much less energy consumption. This, coupled with the general trend of higher charge–discharge capacity of hard carbon materials at least during the first few cycles has made hard carbon an attractive anode material for Li-ion batteries. The extensive research on hard carbon materials concerns a variety of mineral, agricultural and polymeric sources [101-102].

Petroleum coke was one of the non-graphitic materials which received considerable attention in the early 1990s [103]. The performance of petroleum coke was found to be quite comparable with natural graphite. Petroleum coke modified by meso-phase carbon (MPC) coating gave an increase in the reversible capacity [104]. The next classification is meso-phase, pitch-based carbon fibres. These materials show good reversibility [105] and substantial excess lithium up to a ratio of Li_6C_6 can be loaded [106]. Dahn and co-workers [107] have studied the properties of carbonaceous materials prepared from resins. Apart from phenolic resins [108], phenol–formaldehyde resin-based carbonaceous material [109] and PAN-based carbon anodes [110] were also found to give good lithium intercalation efficiency. A number of

disordered-carbon materials have also been prepared from the pyrolysis of polymeric materials such as poly(2-chloro-1-phenylacetylene) [111], poly(vinylchloride) (PVC) [112], condensed poly-nuclear aromatics [113] and indoine blue [114]. Some agricultural-based raw materials such as sugar [115], rice husk [116], coffee beans, green tea, sugarcane [117] and cotton have also been used to prepare active carbon materials and evaluate them for battery applications. Pyrolytic carbon prepared by chemical vapour deposition (CVD) of hydrocarbons was reported [118]. Quite recently, lithium insertion in carbon nanotubes [119] and related materials has received some attention.

1.4.2 Cathode materials

Positive electrode materials for lithium-ion batteries [120] are lithiated oxides that deintercalate Li at an average voltage close to 4V with respect to Li. A systematic study has been proposed for various $LiMO_2$ materials (where M is a transition element), whose structure is composed of a close packing of O^{2-} anions with M and Li in octahedral sites [121]. Simple geometric considerations based on a hard sphere model for the solid show that such $LiMO_2$ materials present the highest volumetric capacities (the quantity of energy available in a given volume of the compound) among other isostructural $LiMX_2$ (X = S, Se, Te) compounds and other MO_2 structures. The order of operating voltages for the reversible Li deintercalation reaction is shown to increase when varying the transition element from 5d to 4d to 3d and from d^n to d^{n+l} (n=0-7).

Compared to $LiMO_2$ (M =Co, Ni), the $LiMn_2O_4$ spine1 presents the advantage of low cost and low toxicity but the drawback of an initially slightly lower capacity and a larger capacity fading upon cycling. These two important characteristics were shown to be strongly influenced by some structural parameters such as the nominal Li/Mn composition and the oxygen stoichiometry [122]. The oxygen stoichiometry of $LiMn_2O_{4-\delta}$ was further investigated, leading to the phase diagram over a wide oxygen-temperature region [123]. A correlation was found [122] between the rate of capacity loss under cycling and the amplitude of the current peak on the voltammogram at 4.5V with respect to Li. As a result, $Li_{1+x}Mn_2O_4$ materials with the best cycling properties can be selected from the simple recording of their voltammogram. Another approach to improve $LiMn_2O_4$ capacity retention upon cycling on the 4V plateau consisted in a doping with monovalent or divalent cations (Li^+, Mg^{2+}, Zn^{2+}) [124]. The improved cyclability, which was gained at the expense of capacity, was attributed to the suppression of the Jahn-Teller effect at the end of discharge as the Mn valence was larger than 3.5.

The specific capacity of orthorhombic $LiMnO_2$, the rapidity of its transformation to spine1 Li_xMnO_2 upon cycling and its cyclability depend on the synthesis conditions. The discrepancies in the reported data are not understood, although some work has been done to try to correlate the electrochemical behavior to structural features. These studies show that it is the combination of the small grain size of the powdered active material used by the battery's electrode and the cationic disorder on both lithium and manganese sites [125], which is responsible for an enhancement of the cycling performance in terms of high capacity and long cycle life [126].

Recent developments of Li-ion batteries have led to the discovery of electrolyte compositions that are highly stable (up to 5V with respect to Li) against oxidation [127]. This increase in the voltage limit allowed some highly oxidative intercalation materials to operate in the 4-5V range. The $LiNiVO_4$ spine1 was found to exhibit a reversible de-intercalation plateau at 4.8V, but with a low capacity of about 40Ah kg^{-1} [128]. Li could be reversibly de-intercalated from the spine1 solid solution $LiCr_yMn_{2-y}O_4$ in two steps (at 4.1 V and at 4.9V with respect to Li), with a 4.9V capacity depending on the Cr content [129].

1.5 Research technique

[130]Apart from charge-discharge curves, a wide variety of electroanalytical techniques are commonly employed to characterise the electrochemical processes which occur at the carbon electrode|electrolyte interface. Slow-scan cyclic voltammetry (SSCV) is used to determine different stages of the intercalation of lithium ions in graphite and the total charge involved in each stage and the potential of charge-discharge [83]. The increase or decrease in the mass during intercalation/de-intercalation is accurately determined by means of an electrochemical quartz crystal microbalance (EQCM) [131]. The interfacial properties of the solid-electrolyte interface (SEI), such as its conductivity and the diffusion rate of ionic species through the interface, are usually determined by employing electrochemical impedance spectroscopy (EIS) [132]. XRD [133] measurements are essentially employed to ascertain the level of intercalation and exfoliation of the graphite lattices on co-intercalation of solvents. The thermal stability of the intercalated carbon material and the decomposition temperatures for processes such as solvent evaporation and lattice transition can be evaluated using thermo-gravimetry (TG). Differential thermal analysis (DTA) provides further information on the exothermicity and endothermicity of the processes involved [134-135]. Scanning electron microscopy (SEM) is extensively used to evaluate the structure of the carbonized material before and after the intercalation processes [136]. The spatial

distribution, such as the surface thickness of different elements, may be evaluated by means of transmission electron microscopy (TEM) [137]. Scanning tunnelling microscopy (STM) has been employed to assess the level of exfoliation caused by different solvents [138]. Atomic force microscopy (AFM) has proved useful in studying the surface transformation as well as the SEI [139]. The structure and composition of the SEI formed on carbon anodes is an important aspect. Aurbach and co-workers [83] have extensively used Fourier transform infrared spectroscopy (FT-IR) to determine the decomposition of the products obtained in different solvents and supporting electrolytes under the operating conditions of Li-ion batteries. The SEI can also be investigated by temperature-controlled gas chromatography (GC) followed by mass spectrum (MS) studies [140]. Raman spectroscopy [141] is adopted to study the roughness of the electrode surface. X-ray photoelectron spectroscopy (XPS) is used to evaluate different atomic level bonding interactions during the intercalation process [142]. The interactions between Li ions and host lattices under different experimental conditions are now being evaluated using ^{7}Li NMR spectroscopy [143-144]. These techniques have been summarized as shown in table1-1.

Table 1-1. Different instrumentation techniques employed for characterization of Li-ion batteries

Analysis	technique	Reference
(I) Electrochemical		
Charge–discharge and cycling efficiency	Charge–discharge curves	–
Stages of intercalation/reversibility/charge	SSCV	[83]
Mass changes during polarisation	EQCM	[131]
Kinetics of intercalated/de-intercalated process	EIS	[83,132]
(II) Diffraction		
Crystallinity of different stages during intercalation	XRD	[133]
(III) Thermal studies		
Thermal stability and thermodynamics of intercalated material	TG and DTA	[134-135]
(IV) Microscopic		
Structural changes in electrode material before and after intercalation	SEM and TEM	[136-137]
Morphological changes at sub-micron level	STM and AFM	[138-139]
(V) Spectroscopy		
Composition of SEI film	FT-IR and GC–MS	[83,140]
Structural disorder of electrode materials	Raman	[141]
Chemical states of intercalants	XPS	[142]
Li-ion binding in carbon lattices	^{7}Li NMR	[143-144]

1.6 The motivation and main issues of this work

Most of the efforts of the development of lithium batteries have been focused on adopting new electrolyte, lithium salt and the electrode materials from a practical side. So it is important and necessary to investigate the mechanism of these problems from the theoretical view point. However the fundamental understanding on the intercalation mechanism of lithium ion on

carbon material electrode (e.g. graphite) is relatively few. The aim of this work is to investigate and to interpret the kinetic process of lithium intercalation on graphite electrode which includes the diffusion of lithium ion from the solution to the electrode surface (electron transfer), the reduction of the lithium ion on electrode surface and the intercalation of the lithium atom in solid graphite (mass transfer).

The main issues in this thesis include: (1)The electrochemical behaviour of lithium ion at pyrolytic graphite electrode. In this part peak currents and potentials of voltammograms of lithium ion at the pyrolytic graphite electrode were obtained under the conventionally voltammetric conditions except for addition of supporting electrolyte. They were interpreted on the basis of the voltammetric concept in order to estimate rate-determining steps and redox potentials at zero current. The cathodic charge evaluated from the integration of the voltammogram was larger by 30% than the anodic one because of side reaction of acetonitrile or impurities. (2) The transition of current of lithium intercalation from solution to graphite. In this part the critical behaviour of lithium intercalation has been found and the time-dependent mass transport theory was developed by use of the Nernst–Planck equation for the solution phase and the diffusion equation for the graphite one. Both equations were combined at the interface through a kind of the Nernst equation which contained a maximum concentration of Li in the graphite predicted from the structure of LiC_6.

1.7 References

[1]Annually updated CRC Handbook of Chemistry and Physics; CRC Press: Boca Raton, FL.

[2] L. Fischer, G. Winkler, G. Jander, Z. Elektrochem. 62 (1958)1.

[3] R. Jasinski, High Energy Batteries; Plenum Press: New York, 1967.

[4] R. Selim, P. Bro, J. Electrochem. Soc. 121(1974)1457.

[5] R.D. Raul, S.B. Brummer, Electrochim. Acta 22(1977)75.

[6] V.R. Koch, J.H. Young, J. Electrochem. Soc. 125(1978)1371.

[7] I. Yoshimatsu, T. Hirai, J. Yamaki, J. Electrochem. Soc. 135(1988)2422.

[8] J. Broadhead, F.A. Trumbore, In Power Sources; Collins, D. H., Ed.; Academic Press: London, 5(1975)661.

[9] M.S. Whittingham, Science 192(1976)1126.

[10] M.S. Whittingham, Prog. Solid State Chem. 12(1978)1.

[11] (a) K. Mizushima, P.C. Jones, P.J. Wiseman, J.B. Goodenough, Mater. Res. Bull. 15(1980)783. (b) K. Mizushima, P.C. Jones, P.J. Wiseman, J.B. Goodenough, Solid State Ionics. 3/4(1981)171.

[12] D.W. Murphy, P. Christian, Science 205(1979)651.

[13] M. Armand, In Materials for Advanced Batteries; Murphy, D. W., Broadhead, J., Steele, B. C. H., Eds.; Plenum Press: New York, 1980; p 145.

[14] K. Xu, Chem. Rev. 104(2004)4303.

[15] M. Lazzari, B. Scrosati, J. Electrochem. Soc. 127(1980)773.

[16] J. Auborn, Y.L. Barberio, J. Electrochem. Soc. 134(1987)638.

[17] K.W. Semkov, A.F. Sammels, J. Electrochem. Soc. 134(1987)766.

[18] B. Scrosati, J. Electrochem. Soc. 139(1992)2776.

[19] T. Nagaura, M. Nagamine, I. Tanabe, N. Miyamoto, Prog. Batteries Sol. Cells 8(1989)84.

[20] T. Nagaura, K. Ozawa, Prog. Batteries Sol. Cells 9(1990)209.

[21] Nishi, Y.; Azuma, H.; Omaru, A. U.S. Patent 4,959,281, 1990.

[22] Ohzhku, T.; Ueda, A.; Nagayama, M. J. Electrochem. Soc. 1993, 140, 1862.

[23] Bittihn, R.; Herr, R.; Hoge, D. J. Power Sources 1993, 43/44, 223.

[24] T. Nagaura, K. Tozawa, Prog. Batt. Solar Cells 9(1990)209.

[25] R. Fong, U. Von Sacken, J.R. Dahn, J. Electrochem. Soc. 137(1990)2009.

[26] M. Broussely, 11th International Meeting on Lithium Batteries, Monterey, CA, June 23-28, 2002; Abstract No. 415; Electrochemical Society: Pennington, NJ.

[27] W.S. Harris, Electrochemical Studies in Cyclic Esters. Ph.D. Thesis, University of California, Berkeley, CA, 1958.

[28] D. Aurbach, M.L. D aroux, P.W. Faguy, E. Yeager, J. Electrochem. Soc. 134(1987)1611.

[29] V.R. Koch, J.H. Young, J. Electrochem. Soc. 125(1978)1371.

[30] V.R. Koch, J.L. Goldman, C.J. Mattos, M. Mulvaney, J. Electrochem. Soc. 129 (1982)1.

[31] K.M. Abraham, J.L. Goldman, D.L. Natwig, J. Electrochem. Soc. 129 (1982)2404.

[32] F.W. Dampier, J. Electrochem. Soc. 128 (1981)2501.

[33] K.M. Abraham, D.M. Pasquariello, F.J. Martin, J. Electrochem. Soc. 133(1986)661.

[34] I. Yoshimatsu, T. Hirai, J. Yamaki, J. Electrochem. Soc. 135(1988)2422.

[35] K.M. Abraham, J.S. Foos, J.L. Goldman, J. Electrochem. Soc. 131(1984)2197.

[36] V.R. Koch, J. Electrochem. Soc. 126(1979)181

[37] J.S. Foos, T.J. Stolki, J. Electrochem. Soc. 135(1988)2769.

[38] Y. Geronov, B. Puresheva, R.V. Moshtev, P. Zlatilova, T. Kosev, Z. Staynov, G. Pistoia, M. Pasquali, J. Electrochem. Soc. 137 (1990)3338.
[39] W. Elliott, Report No. 1, Contract NAS 3-6015 (N 65-11518), Sept 1964.
[40] G. Pistoia, J. Electrochem. Soc. 118(1971)153.
[41] S. Subbarao, D.H. Shen, F. Deligiannis, C.K. Huang, G. Halpert, J. Power Sources. 29(1990)579.
[42] N. Takami, T. Ohsaki, K. Inada, J. Electrochem. Soc. 139(1992)1849.
[43] M. Arakawa, S. Tobishima, T. Hirai, J. Yamaki, J. Electrochem. Soc. 133(1986)1527.
[44] S. Surampudi, D.H. Shen, C.K. Huang, S.R. Narayanan, A. Attia, G. Halpert, E. Peled, J. Power Sources. 43/44(1993)21.
[45] S. Tobishima, M. Arakawa, T. Hirai, J. Yamaki, J. Power Sources. 26(1989)449.
[46] R.S. McMillan, M.W. Juskow, J. Electrochem. Soc. 138(1991)1556.
[47] J. Yamaura, Y. Ozaki, A. Morita, A. Ohta, J. Power Sources 43/44(1993)233.
[48] S.S. Zhang, Q.G. Liu, L.L. Yang, J. Electrochem. Soc. 140(1993)L107.
[49] D. Guyomard, J. M. Tarascon, J. Electrochem. Soc. 139(1992)937.
[50] J.M. Tarascon, D .Guyomard, G.L. Baker, J. Power Sources. 43/44(1993)689.
[51] W. Ebner, D. Fouchard, L. Xie, Solid State Ionics. 69(1994)238.
[52] J. Dahn, U. Von Sacken, M.W. Juzkow, H. Al-Janaby, J. Electrochem. Soc. 138(1991)2207.
[53] T. Ohzuku, Y. Iwakoshi, K. Sawai, J. Electrochem. Soc. 140(1993)2490.
[54] S.Y. Huang, L. Kavan, I. Exnar, M. Grätzel, J. Electrochem. Soc. 142(1995)L142.
[55] D. Guyomard, J. Tarascon, M. J. Electrochem. Soc. 140(1993)3071.
[56] J.M. Tarascon, D. Guyomard, Solid State Ionics. 69(1994)293.
[57] T. Zheng, Y. Liu, E.W. Fuller, S. Tseng, U. Von Sacken, J. Dahn, J. Electrochem. Soc. 142(1995)2581.
[58] M. Morita, T. Ichimura, M. Ishikawa. Y. Matsuda, J. Electrochem. Soc. 143(1996)L26.
[59] Y. Ein-Eli, S.R. Thomas, R. Chadha, T.J. Blakley, V.R. Koch, J. Electrochem. Soc. 144(1997)823.
[60] A.C. Chu, J.Y. Josefowicz, G.C. Farrington, J. Electrochem. Soc. 144(1997)4161.
[61] D. Aurbach, Y. Ein-Eli, B. Markovsky, A. Zaban, S. Luski, Y. Carmeli, H. Yamin, J. Electrochem. Soc. 142(1995)2882.
[62] I. Koetschau, M.N. Richard, J.R. Dahn, J.B. Soupart, J.C. Rousche, J. Electrochem. Soc. 142 (1995)2906.

[63] E. Peled, D. Golodnitsky, C. Menachem, D. Bar-Tow, J. Electrochem. Soc. 145(1998)3482.
[64] Y. Ein-Eli, S.R. Thomas, V.R. Koch, D. Aurbach, A. Schecheter, B. Markovsky, J. Electrochem. Soc. 143(1996)L273.
[65] Y. Ein-Eli, S.F. McDevitt, D. Aurbach, B. Markovsky, A. Schecheter, J. Electrochem. Soc. 144(1997)L180.
[66] K. Sekai, H. Azuma, A. Omaru, S. Fujita, H. Imoto, T. Endo, K. Yamaura, Y. Nishi, J. Power Sources. 43/44(1993)241.
[67] R. Jasinski, S. Carroll, J. Electrochem. Soc. 117(1970)218.
[68] I. Uchida, H. Sato, J. Electrochem. Soc. 142(1995)L139.
[69] R.D. Rauh, T.F. Reise, S.B. Brummer, J. Electrochem. Soc. 125(1978)186.
[70] E. Plichta, S. Slane, M. Uchiyama, M. Salomon, D. Chua, W.B. Ebner, H.W. Lin, J. Electrochem. Soc. 136(1989)1865.
[71] K.Takata, M. Morita, Y. Matsuda, J. Electrochem. Soc. 132(1985)126.
[72] S.S. Zhang, K. Xu, T.R. Jow, J. Electrochem. Soc. 149(2002)A586.
[73] S.S. Zhang, K. Xu, T.R. Jow, J. Solid State Electrochem. 7(2003)147.
[74] A. Webber, J. Electrochem. Soc. 138(1991)2586.
[75] L.J.Krause, W. Lamanna, J. Summerfield, M. Engle, G. Korba, R. Loch, R. Atanasoski, J. Power Sources. 68(1997)320.
[76] C.W. Walker, J.D. Cox, M. Salomon, J. Electrochem. Soc. 143(1996)L80.
[77] Y. Sasaki, M. Handa, K. Kurashima, T. Tonuma, K. Usami, J. Electrochem. Soc. 148(2001)A999.
[78] W. Xu, A. Shusterman, M. Videa, V. Velikov, R.L. Marzke, C.A. Angell, J. Electrochem. Soc. 150(2003)E74.
[79] M. Schmidt, U. Heider. A. Kuehner, R.Oesten, M. Jungnitz, N. Ignat'ev, P. Sartori, J. Power Sources. 97/98(2001)557.
[80] J.S. Gnanaraj, E. Zinigrad, M.D. Levi, D. Aurbach, M. Schmidt, J. Power Sources. 119/121 (2003)799.
[81] T.J. Barbarich, P.F. Driscoll, Electrochem. Solid-State Lett. 6(2003)A113.
[82] M. Endo, C. Kim, K. Nishimura, T. Fujino, K. Miyashita, Carbon. 38(2000)183.
[83] D. Aurbach, B. Markovsky, I. Weissman, E. Levi, Y.E. Eli, Electrochim. Acta. 45(1999)67.
[84] R. Yazami, J. Power Sources. 97/98(2001)33.
[85] S. Basu, J. Power Sources. 82(1999)200.

[86] F. Funabiki, M. Inaba, Z. Ogumi, J. Power Sources. 68(1997)227.
[87] Y. Korai, S. Ishida, S.H. Yoon, I. Mochida, Y. Nakagawa, C.Y.Matsumura, Y. Sakai, M. Komatu, Carbon. 35(1999)1503.
[88] W. Xing, J.R. Dahn, J. Electrochem. Soc. 144(1997)1195.
[89] C. Yuqin, L. Hong, W. Lie, L. Tianhong, J. Power Sources. 68(1997)187.
[90] K. Tatsumi, K. Zaghib, Y. Sawada, H. Abe, T. Ohsaki, J. Electrochem. Soc. 142(1999)1090.
[91] Y. Sato, T. Nakano, K. Kobayakawa, T. Kawai, A. Yokoyama, J. Power Sources. 75(1998)271.
[92] Q.-M. Pan, Z.-H. Deng, X.-Z. Zhang, G.-X. Wan, J. Power Sources. 79(1999)25.
[93] H. Wang, T. Ikeda, K. Fukuda, M. Yoshio, J. Power Sources. 83(1999)141.
[94] T. Takamura, M. Saito, A. Shimokawa, C. Nakahara, K. Sekine, S. Maeno, N. Kibayashi, J. Power Sources. 90(2000)45.
[95] S. Yoon, H. Kim, S.M. Oh, J. Power Sources. 94(2001)68.
[96] S.B. Ng, J.-Y. Lee, Z.L. Liu, J. Power Sources. 94(2001)63.
[97] A.M. Wilson, J.R. Dahn, J. Electrochem. Soc. 142(1995)327.
[98] M. Endo, C. Kim, T. Karaki, Y. Nishimura, M.J. Mattew, S.D.M. Brown, M.S. Dresselhaus, Carbon. 37(1999)561.
[99] J.-Y. Lee, R. Zhang, Z. Liu, J. Power Sources. 90(2000)70.
[100] T. Takamura, K. Sumiya, J. Suzuki, C. Yamada, K. Sekine, J. PowerSources. 81/82(1999)368.
[101] D. Aurbach (Ed.), Non-Aqueous Electrochemistry, Marcel Dekker, New York, 1999.
[102] J.R. Dahn, T. Zheng, Y. Liu, J.-S. Xue, Science. 270(1995)590.
[103] R. Fong, U. von Sacken, J.R. Dahn, J. Electrochem. Soc. 137(1990)2009.
[104] G. Okuna, K. Kobayakawa, Y. Sato, T. Kawai, A. Yokoyama, DenkiKagak. 65(1997)226.
[105] R. Yazami, K. Zaghib, M. Deschamps, J. Power Sources. 52(1994)55.
[106] M. Deschamps, R. Yazami, J. Power Sources. 68(1997)236.
[107] Y. Liu, J.-S. Xue, T. Zheng, J.R. Dahn, Carbon. 34(1996)193.
[108] T. Takamura, H. Awano, T. Ura, K. Sumiya, J. Power Sources. 68(1997)114.
[109] B. Huang, Y. Huang, Z. Wang, L. Chen, R. Xue, F. Wang, J. Power Sources. 58(1996)231.
[110] M.W. Verbrugge, B.J. Koch, J. Electrochem. Soc. 143(1996)24.
[111] R. Kanno, Y. Takeda, T. Ichikawa, R. Nakanishi, O. Yamamoto,J. Power Sources 26(1989)535.

[112] T. Zheng, J.R. Dhan, J. Power Sources. 68(1997)201.
[113] K. Tokumistsu, A. Mabuchi, H. Fujumoto, T. Kasuh, J. Electrochem.Soc. 43(1996)2235.
[114] L. Duclaux, E. Frackowiak, F. Beguin, J. Power Sources. 81/82(1999)323.
[115] W. Xing, J.-S. Xue, J.R. Dahn, J. Electrochem. Soc. 143(1996)3046.
[116] G.T.K. Fey, C.-L. Chen, J. Power Sources. 97/98(2001)47.
[117] S.-I. Yamada, H. Imoto, K. Sekai, M. Nagamine, Proceedings of the Electrochemical Society Spring Meeting, Montreal, Quebec,Canada, May 1997, The Electrochemical Society Inc., Pennington, NJ, Extended Abstracts, Vol. 97-1, p. 85.
[118] M. Mohri, N. Yanagiasawa, T. Tajima, H. Tanaka, T. Mitate, S. Nakajima, M. Yoshida, Y. Yoshimoto, T. Suzuki, H. Wada, J. Power Sources. 26(1989)545.
[119] F. Leroux, K. Meternier, S. Gautier, E. Frackowiak, S. Bonnamy,F. Beguin, J. Power Sources. 81/82(1999)317.
[120] G. Ouvrard, D. Guyomard, Current Opinion in Solid State & Materials Science. 1(1996)260.
[121] T. Ohzuku, A. Ueda, Solid State lonics. 69(1994)201.
[122] J.M. Tarascon, W.R. McKinnon, F. Coowar, T.N. Bowmer, G. Amatucci, D. Guyomard, J electrochem Soc. 141(1994)1421.
[123] A. Yamada, K. Miura, K. Hinokuma, M. Tanaka, J Electrochem Soc. 142(1995)2149.
[124] R. J. Gummow, A. De Kock, M.M. Thackeray, Solid State lonics. 69(1994)59.
[125] L. Croguennec, P. Deniard, R. Brec, A. Lacert, J Mater Chem. 5(1995)1919.
[126] L. Croguennec, P. Deniard, R. Brec, A. Lecerf, Solid State lonics. 89 (I 996)127.
[127] D. Guyomard. J.M. Tarascon, Solid State lonics. 69(1994)293.
[128] G.T.K. Fey, W. Li, J.R. Dahn, J Electrochem Soc. 141(1994)2279.
[129] C. Sigala, D. Guyomard, A. Verbaere, Y. Piffard, M.Tournoux, Solid State lonics. 81(1995)167.
[130] M. Noel, V. Suryanarayanan, Journal of Power Sources 111(2002)193.
[131] M. Morita, T. Ichimura, M. Ishikawa, Y. Matsuda, J. Power Sources 68 (1997) 253.
[132] T. Piano, S.-M. Park, C.-H. Don, S.-I. Moon, J. Electrochem. Soc. 146(1999)2794.
[133] A. Hamwi, Ph. Touzain, C. Reikel, Synth. Met. 7(1983)23.
[134] R. Santhanam, M. Noel, J. Power Sources. 66(1997)47.
[135] Y. Maeda, Ph. Touzain, Electrochim. Acta. 33(1988)1493.
[136] K. Suzuki, T. Iijima, M. Wakihara, Electrochim. Acta. 44(1999)2185.
[137] G.T. Wu, C.S. Wang, X.B. Zhang, H.S. Yang, Z.F. Qi, P.M. He, W.Z. Li, J. Electrochem.

Soc. 146(1999)1696.
[138] M. Inaba, Y. Kawatte, A. Funabiki, S.K. Jeong, T. Abe, Z. Ogumi, Electrochim. Acta. 45(1999) 99.
[139] F. Kong, R. Kostecki, G. Nadeau, X. Song, K. Zaghib, K. Kinoshita, F. McLarnon, J. Power Sources. 97/98(2001)58.
[140] Z. Ogurni, A. Sano, M. Inaba, T. Abe, J. Power Sources. 97/98(2001) 156.
[141] J.C. Panitz, P. Novak, J. Power Sources. 97/98(2001) 174.
[142] D. Bar-Tow, E. Peled, L. Burstein, J. Electrochem. Soc. 146(1999)824.
[143] K. Tatsumi, T. Akai, T. Imamura, K. Zaghib, N. Iwashita, S. Higuchi, Y. Sawada, J. Electrochem. Soc. 143(1996)1923.
[144] K. Zaghib, K. Tatsumi, Y. Sawada, S. Higuchi, H. Abe, T. Ohsaki, J. Electrochem. Soc. 146(1999)2784.

Chapter 2

Interpretation of voltammograms of lithium ion at pyrolytic graphite electrode

2.1 Introduction

The principle of lithium rechargeable batteries at graphite anodes lies in the intercalation of lithium ion into graphite layers and the de-intercalation of the intercalated lithium to the solution [1–8]. The former is caused by the cathodic reaction of Li^+ at less negative potential than the standard potential of $Li^+|Li$ owing to the stabilization of Li into several graphite stages by the intercalation [3,4,9]. The latter is the anodic dissolution of the intercalated lithium at more positive potential by 0.5–1.3 V than the intercalation potential [10–12]. Although the lithium batteries have practically reversible with good cycleability, the potential difference between the intercalation and the de-intercalation is much larger than that of voltammetrically reversible reaction. The irreversibility is also found in the cathodic charge larger than the anodic charge [10,12–14]. These complications obviously degrade the efficiency and the life of lithium batteries. The intercalation and the deintercalation have frequently been observed under kinetic conditions rather than static conditions like potentiometry. Even basic experiments of graphite anodes have been made at large current, high concentration of lithium ions and a large electrode area without adding supporting electrolyte. Consequently, experimental values depend so strongly on conditions and techniques that they vary from laboratory to laboratory. A strategy of minimizing of the complications is to decrease concentrations of lithium ion. Then it might yield values close to thermodynamic quantities such as the standard potential of the intercalation. However, charge interaction among lithium ions cannot be prevented from voltammograms because there exists, in principle, no supporting electrolyte for the lithium ion systems. This paper aims at analyzing voltammetric peaks of lithium ion at graphite electrodes and determining peak potentials almost independent of techniques and experimental artifacts. A key of the analysis results in subtracting migration effects from the currents and the solution resistance from the observed potentials.

2.2 Experimental

All the chemicals were of analytical grade. Acetonitrile was treated with molecular sieves 4A1/8 (Wako, Tokyo) in order to remove moisture. All the solutions were bubbled with highly purified nitrogen before voltammetric run. Cyclic voltammetry was performed with a

Potentio/Galvanostat (Model 1112, Huso, Kawasaki) under the control of a computer at room temperature in a three-electrode cell. The pyrolytic graphite electrode (PGE) (BAS Inc, Tokyo) and the glassy carbon electrode (GCE) (BAS Inc, Tokyo) 3 mm in diameter were used as working electrodes. A platinum coil and a Ag|AgxO were used as the counter and the reference electrodes, respectively. The potential at the Ag|AgxO was by 0.054 V lower than that at Ag|AgCl. The working electrode was polished with 0.05 μm alumina paste on wetted cotton and rinsed with acetonitrile in the ultrasonic bath for 1 min before each voltammetric run. The crystallinity of graphite electrode was investigated by Raman spectroscopy (JASCO, NRS-1000) with an Ar-ion laser (excitation line 514.5 nm, 0.2 mW), objective 50×(numerical aperture 0.75).

2.3 Results and discussion

Fig. 2-1 shows the Raman spectra of the PGE electrode immediately after polishing (curve (a)) and after 15 potentiodynamic intercalation–deintercalation cycles (curve (b)). There is a sharp band at 1580 cm^{-1} and a faint band at about 1350 cm^{-1} on curve (a). The sharp band at 1580 cm^{-1} has been assigned to Raman active E_{2g} mode frequency [40], known as the G band, associated with in plane symmetric C–C stretches. Carbonaceous materials with high degree of graphitization usually give a strong peak at 1580 cm^{-1}. Polycrystalline graphite and disordered carbons have exhibited a band at about 1350 cm^{-1} (A_{1g} mode, D band) due to finite crystalline sizes and imperfection of carbonaceous materials [41]. From curve (a) we can conclude that the structure of the electrode is not destroyed with the polishing but does keep good crystallinity. The decrease in the band at 1580 cm^{-1} indicates that the crystallinity was lost after the lithium ions intercalation.

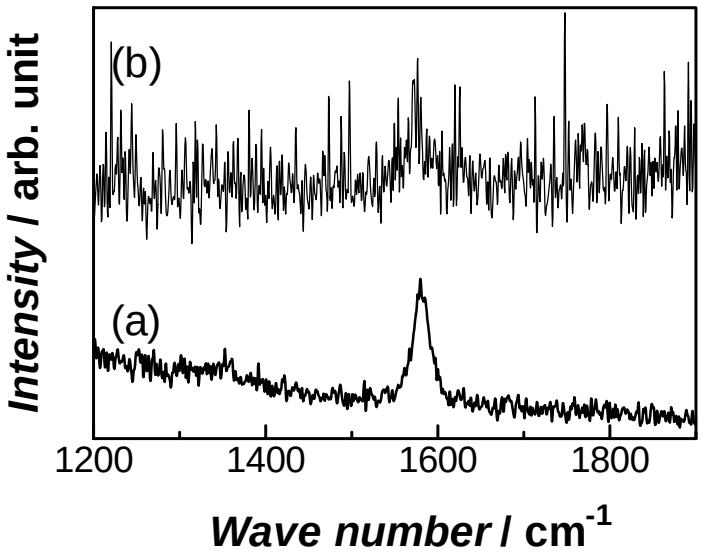

Fig 2-1. Raman spectra of a PGE (a) immediately after polishing and (b) after 15 potentiodynamic intercalation-deintercalation cycles in 3 mM $LiClO_4$ in acetonitrile at room temperature.

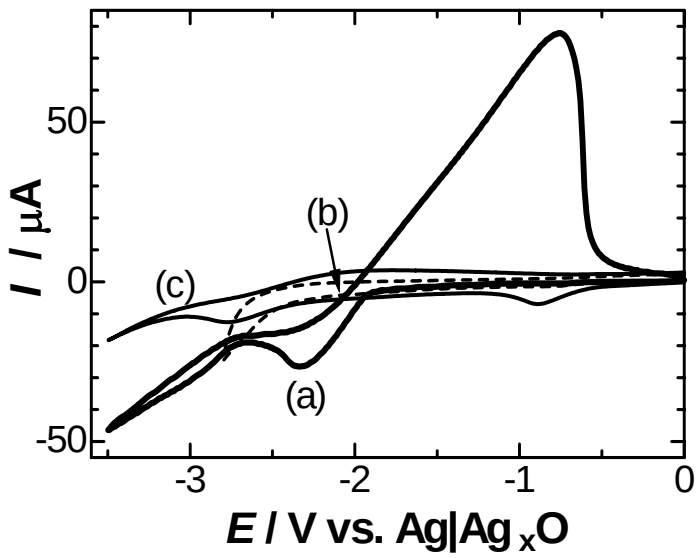

Fig 2-2. Cyclic voltammograms of 0.76 mM $LiClO_4$ at v = 50 mV s^{-1} in acetonitrile at the PGE without (a) and with (c) oxygen and moisture, and at the GCE without (b) oxygen and moisture.

Fig. 2-2 shows the voltammogram of 0.76 mM $LiClO_4$ at the PGE (curve (a)) in acetonitrile after removing oxygen and moisture. The voltammogram did not vary with the number of potential cycles. The cathodic wave appeared at ca -2.4 V. The GCE instead of the PGE showed no wave at this potential (curve (b)). The cathodic wave, being specific to the PGE, can be attributed to the intercalation of lithium ions into the graphite. The shoulder of the cathodic wave at -3.0 V can be attributed either to the ordinary reduction of Li^+ to Li or to the reduction of acetonitrile. Since the concentration of lithium ion on the PGE surface at E < -2.5 V is actually zero owing to the limiting current, the further reduction of lithium ion is not be predicted. Therefore, the shoulder is ascribed to the reduction of acetonitrile at the intercalated PGE surface, as will be described in the latter section.

The anodic wave with a peak at -0.8 V is caused by the de-intercalation, because it cannot be observed at the GCE which exhibited no intercalation [17,42–45]. The anodic peak potential reported varied largely with the current from -1.7 to -0.8 V [12,15], owing to large electric resistance of the solution. The disappearance of the anodic current at E > -0.5 V indicates the exhaustive dissolution of the intercalated lithium to the solution bulk.

When the solution was not deaerated and not dried, the voltammogram at the PGE showed (curve (c)) two cathodic waves at -0.9 and -2.8 V and the broad anodic wave at -2.0 V. Since the cathodic wave at -0.9 V disappeared by deaeration of the solution, it is caused by the reduction of oxygen or oxygen-containing surface groups at the electrode [16,17]. Oxygen and water suppressed the intercalation and the de-intercalation currents [18], and shifted the intercalation potential in the negative direction.

Fig. 2-3 shows the dependence of cathodic peak current, $I_{p,c}$, on the concentration, c, of

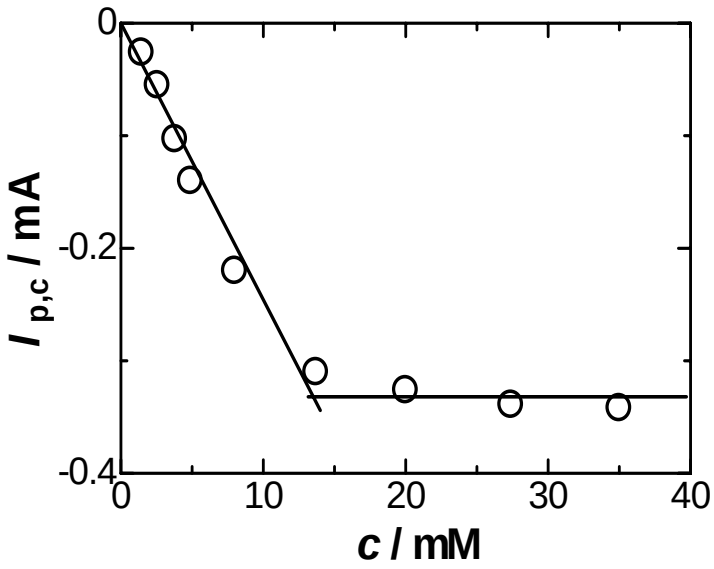

Fig 2-3. Variation of the cathodic peak current, $I_{p,c}$ with the concentration of the $LiClO_4$ in deaerated and dried acetonitrile at $v = 50$ mV s^{-1}.

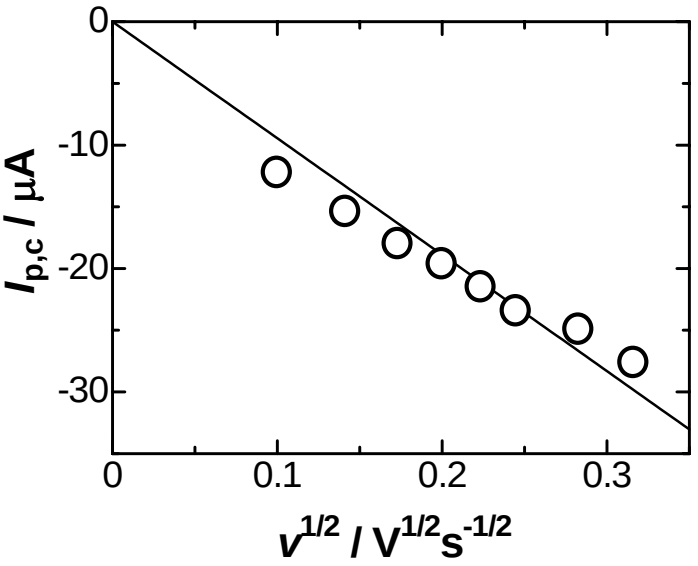

Fig 2-4. Variation of the cathodic peak current, $I_{p,c}$, with square root of scan rate, $v^{1/2}$, in 1.45 mM Li ClO_4 in acetonitrile.

$LiClO_4$. The current for c > 25 mM was almost independent of *c*. It should be controlled by slower processes than the supply of lithium ion. The slower processes are possibly the charge transfer step of Li^+ in the graphite [8–30] and mass transport of the reaction product (Li) into the graphite [19,23–32]. In contrast, the proportionality at low concentrations indicates that the current should be controlled by diffusion of Li^+ or the first order kinetics with respect to *c*. The behavior in this domain can be analyzed by means of usual voltammetric techniques, and hence our concern is directed to the proportional domain.

In order to find the rate-determining step in the proportional domain of the $I_{p,c}$ vs. *c* variation, we examined dependence of the peak current on the potential scan rate, *v*. The increase in *v* enhanced $I_{p,c}$, and shifted the cathodic peak potential in the negative direction. Fig 2-4 shows the dependence of the cathodic peak current, $I_{p,c}$, on $v^{1/2}$, exhibiting the approximate proportionality. Proportionality implies a diffusion-controlled process of a reactant in solution. Since the solution contains only $LiClO_4$ without supporting electrolyte, the approximate proportionality infers that the current is controlled not only by diffusion but also by

electric migration. The theory of the current controlled by both diffusion and migration has been developed in detail for the steady-state voltammogram at a microelectrode [33–35]. However, the assumptions in the theory are not realized in usual experiments because of a leak of ions from a reference electrode, formation of ions at a counter electrode, and difficulty of realizing the model of cell geometry and electrode geometry. Therefore, analysis of the migration current becomes necessarily semi-quantitative. When a reactant has single charge and a product has no charge, the limiting current value is reported to be twice the value without migration [34]. Applying this concept to the cathodic peak current without supporting electrolyte, we get approximately,

$$I_p = (0.446 \times 2) FcA(FDv/RT)^{1/2} \qquad (1)$$

where A is the area of the PGE, D is the diffusion coefficient of Li^+ in the solution, and F, R, and T have the conventional meanings. From the known values of c, A and $I_{p,c}v^{-1/2}$, we estimated the diffusion coefficient to be 3×10^{-5} cm^2 s^{-1}. It is close to the value 2.4×10^{-5} cm^2 s^{-1} for ferrocene in acetonitrile. Therefore, the cathodic peak current is controlled both by diffusion and migration of Li^+ in the solution rather than the kinetics of the intercalation. The value of D is not so accurate that one digit may be allowed, not only because of involvement of approximation in Eq. (1) with respect to migration but also because of the assumption of the reversible reaction. We attempted to obtain a diffusion-controlled cathodic peak current at the platinum electrode and the GCE, but failed owing to exponentially rising current. Reported values of D for lithium batteries are 4.7×10^{-6} cm^2 s^{-1} in the mixture of ethylene carbonate and ethylene methylene carbonate [36] and 3×10^{-6} cm^2 s^{-1} in propylene carbonate [37].

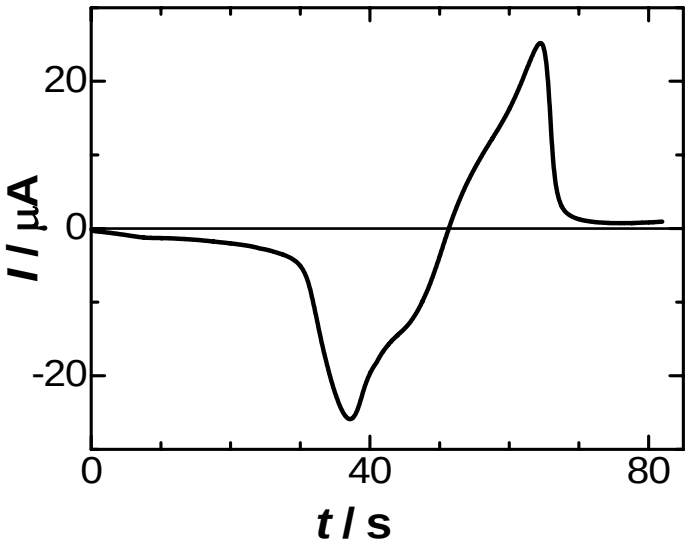

Fig 2-5. Current-time curve converted from the cyclic voltammogram of 1.45mM $LiClO_4$ acetonitrile solution at v = 50 mV s^{-1}.

The anodic wave, which can be attributed to the de-intercalation, may behave as an adsorption wave because the process of the intercalation and the de--intercalation resembles mechanistically that of pre-electrolysis

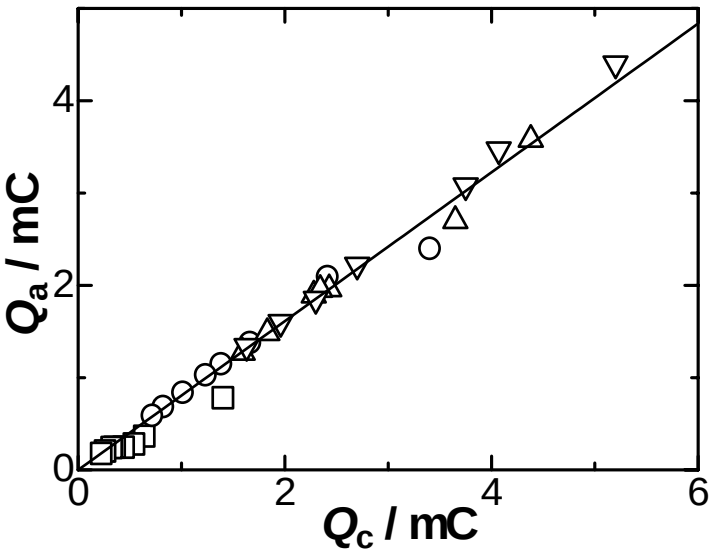

Fig 2-6. Dependence of the anodic charge, Q_a, on the cathodic charge, Q_c, at different scan rates ($10 < v < 100$ mV s^{-1}) in 0.48 (squares), 2.56 (circles), 3.8 (upper triangles), and 4.9 mM (lower triangles) $LiClO_4$ solutions in acetonitrile.

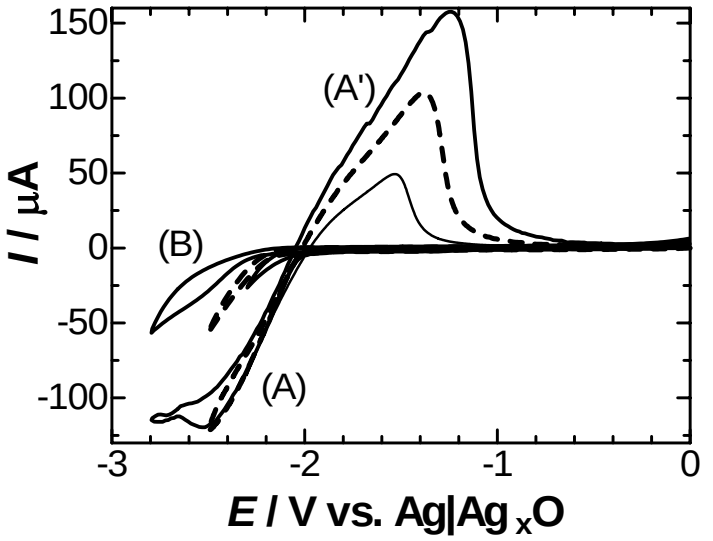

Fig 2-7. Cyclic voltammograms at the (A,A') PGE and at the (B) GCE when the potential was reversed at -2.3, -2.5 and -2.8 V in 4.9 mM $LiClO_4$ acetonitrile solution at $v = 50$ mV s^{-1}.

and dissolution in stripping voltammetry. In order to confirm the properties of a surface wave for the anodic peak current, we applied -2.7 V for 20 s and then scanned the potential in the positive direction at various scan rates. The peak current was unexpectedly not proportional to the scan rate although the voltammogram exhibited no diffusion tail at $E > -0.2$ V after the peak. The deviation from the proportionality is ascribed to the deformation of the anodic wave, associated with positive potential shift with an increase in the current. A strategy of confirming the anodic wave to be a surface wave is to compare the anodic charge with the cathodic one.

We evaluated the two kinds of the charge by integrating the current with respect to the electrolysis time after the voltammogram was redrawn to the current–time curve, as is shown in Fig 2-5. Both the cathodic charge, Q_c, and the anodic one, Q_a, were increased proportionally with an increase in the concentration of lithium ion, whereas they decreased with an increase in the scan rate.

Q_a was proportional to Q_c for $v > 20$ mV s^{-1} and for various values of $c < 5$ mM, as is shown in Fig 2-6. The proportionality implies that the degree of the charge

compensation is independent of c and v. However, the compensation is not maintained, demonstrated quantitatively by Q_c = 1.24Qa. Since Q_a means the accumulated charge, the amount of 24% cathodic charge turns to be lost. The charge loss has been reported to be 67%, 130% and 160% in dimethyl sulfoxide, propylene carbonate and dimethyl formamide at the polypropylene–graphite composite electrode [10]. It has varied complicatedly with mixture of solvents [14].

Table 2-1. Dependence of ratios of Q_c at the GCE to Q_c at the PGE on reverse potentials, E_r

E_r / V	-2.1	-2.2	-2.3	-2.4	-2.5	-2.6	-2.7	-2.8
Q_c(GCE)/ mC	0.028	0.077	0.153	0.265	0.392	0.480	0.520	0.600
Q_c(GCE)/Q_c(PGE)	0.30	0.30	0.29	0.30	0.30	0.28	0.25	0.23

The cathodic decomposition of solvents seems to decrease the charge compensation. In order to confirm the participation in the decomposition of acetonitrile, we obtained the cathodic charge at the PGE and the GCE from the integration of voltammograms by altering negative reverse potentials, E_r, as is shown in Fig 2-7. The cathodic charge increased with the negative shift of E_r, as is shown in Table2-1. The ratio of the charge at the GCE to that at the PGE was almost 0.30, independent of E_r. Since the GCE does not provide intercalation, the cathodic charge at the GCE is ascribed to reduction of impurities included in acetonitrile or of acetonitrile itself. The ratio is close to the charge loss (24%) in Fig 2-6. Therefore, the charge loss is not caused by reaction of lithium but is attributed to the decomposition of impurities or acetonitrile.

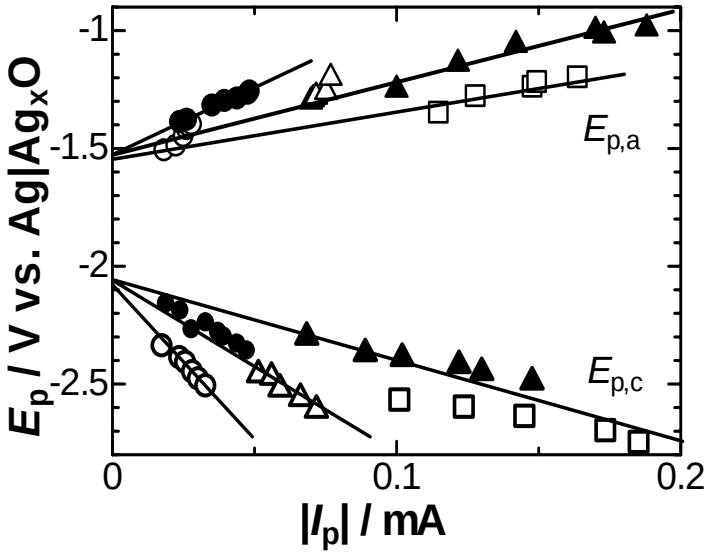

Fig 2-8. Variations of $E_{p,c}$ (in the lower half) with $I_{p,c}$ and $E_{p,a}$ (in the upper half) with $I_{p,a}$ in 0.48 (full circles), 1.45 (open circles), 2.56 (open triangles), 3.8 (full triangles) and 4.9 mM (squares) $LiClO_4$ acetonitrile solutions at different scan rates.

Although the voltammetric current and charge have been now interpreted approximately, a serious problem still lies in large variations of peak potentials with experimental conditions. Actually, characteristic

potentials vary from laboratory to laboratory. We consider that the main reason is due to electric resistance (*IR*-drop) of the solution because of including no supporting electrolyte. Since a potential shift by the *IR*-drop should have a linear variation of the current, we plotted $E_{p,a}$ and $E_{p,c}$ against $I_{p,a}$ and $|I_{p,c}|$ in Fig 2-8 for various values of v at a given concentration, where E_p stands for $E_{p,a}$ or $E_{p,c}$, and I_p stands for $I_{p,a}$ or $|I_{p,c}|$. Data of (E_p, I_p) at each concentration fall on a straightline, suggesting the potential shift by the *IR*-drop. The values of E_p extrapolated to $I_p \rightarrow 0$ for different concentrations merge in $(E_{p,a})_{I=0}$ = -1.53±0.05 V or -1.58 V vs. Ag|AgCl and $(E_{p,c})_{I=0}$ =-2.06±0.05 V or -2.11 V vs. Ag|AgCl. These values are peak potentials without including the *IR*-drop. The difference in the peak potentials, $(E_{p,a})_{I=0}$ -$(E_{p,c})_{I=0}$, is 0.53 V,. This energy is an interfacial kinetic contribution of the intercalation and/or the de-intercalation, and hence is lost at a cycle of the charge/discharge. A technique of reducing this voltage should be an important subject of improving energetic efficiency of lithium batteries.

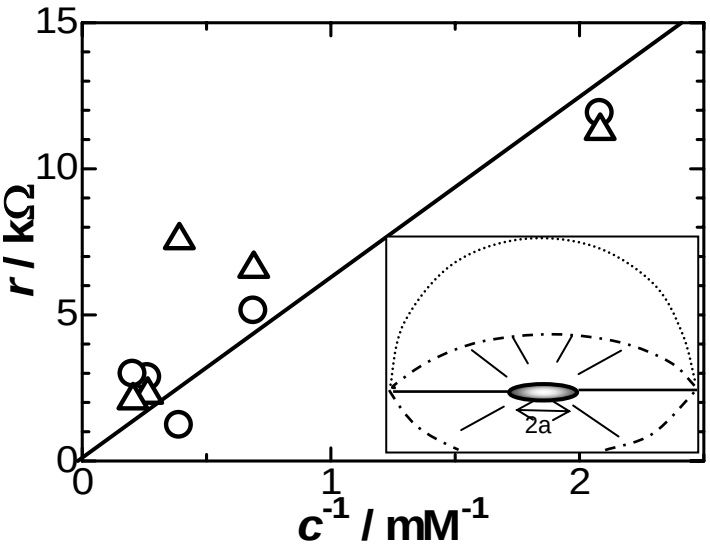

Fig 2-9. Dependence of the absolute values of slopes in Fig 2-8 for the anodic (triangles) and the cathodic (circles) waves on the inverse of the concentration of $LiClO_4$. The inset is the model of estimating the electric resistance in the solution when the disk electrode is covered with the large dome of the counter electrode.

Slopes of the lines in Fig 2-8 have dimension of electric resistance, *r*. The absolute values of the slopes increased with a decrease in the concentration. Since they may correspond to solution resistance, we plotted them against the inverse concentration of $LiClO_4$ in Fig 2-9. Although the plots are rather scattered, they show a proportional relation, common to the anodic waves and the cathodic waves. Therefore *r* means the solution resistance. The slope is 6 ΩM. We consider an electric resistance model (inset of Fig 2-9) in the cell at which a disk electrode *a* in radius is located flush on a large planar insulator in a medium with the molar conductivity, Λ_m. When the medium is covered with a large dome of a counter electrode, the resistance between the counter electrode and the disk electrode is given by [38]:

$r = 1/4c\Lambda_m a$, (2)

where Λ_m is the sum of limiting ionic conductivity of Li^+ and ClO^{-4} . Since no data of the conductivity in acetonitrile are available unfortunately, we use values in water, Λ_m = (3.84 + 6.73) $\times 10^{-3}$ S m^2 mol^{-1} [39]. If we take c to be the bulk concentration of $LiClO_4$, the value of rc is 16 ΩM. This value is three-times larger than the experimental one (6 ΩM). We have to be satisfied with only the agreement of the order of magnitude partly because of the rough model in cell geometry, partly because of the use of the Λ_m values for water, and partly because of the disregard of mass transport of Li^+ and ClO^{-4} associated with the charge transfer. The practical method of subtracting the *IR*-drop contribution is to plot *E* against *I* and to extrapolate *I* to zero.

2.4 Conclusion

Voltammograms of $LiClO_4$ in dried and deaerated acetonitrile showed the diffusion–migration controlled cathodic peak current and the adsorption-controlled anodic current when the concentration was less than 20 mM. The former is caused by the intercalation of Li^+ into the PGE, but the current is controlled by the mass transport of Li^+ in acetonitrile. It is not easy to evaluate the current accurately enough for in conventional voltammetry, because of complicated analysis of the migration current, involvement of impurity of salt, insufficient data of the diffusion coefficient and the conductivity, the irreversible reaction, and reduction of solvent. The cathodic charge was larger by 30% than the anodic one owing to the reduction current of acetonitrile or impurities in the solvent. The reduction of solvent is responsible for the charge loss in the charge–discharge cycle. The potential shift caused by the *IR*-drop was corrected with the extrapolation of *I* to zero in the plot of *E vs. I*. Then there was 0.53 V potential difference between the intercalation and the de-intercalation. This value, corresponding to 51 kJ mol^{-1}, is the energy lost inevitably at each charge/discharge cycle.

2.5 References

[1] S. Megahed, W. Ebner, J. Power Sources 54(1995)155.

[2] R. Fong, U. Von Sacken, J.R. Dahn, J. Electrochem. Soc. 137(1990)2009.

[3] J.R. Dahn, A.K. Sleigh, Hang Shi, J.N. Reimers, Q. Zhong, B.M. Way, Electrochim. Acta 38(1993)1179.

[4] T. Zheng, J.N. Reimers, J.R. Dahn, Phys. Rev. B 51(1995)734.

[5] S. Lemont, D. Billaud, J. Power Sources 54(1995)338.

[6] A. Funabiki, M. Inaba, Z. Ogumu, J. Power Sources 68(1997)227.
[7] D. Aurbach, A. Zaban, Y. Ein-Eli, I. Weissman, O. Chusid, B. Markovsky, M. Levi, E. Levi, A. Schechter, E. Granot, J. Power Sources 68(1997)91.
[8] M.D. Levi, D. Aurbach, Electrochim. Acta 45(1999)167.
[9] D. Aurbach, B. Markovsky, I. Weissman, E. Levi, Y. Ein-Eli, Electrochim. Acta 45(1999)67.
[10] R. Santhanam, M. Noel, J. Power Sources 66(1997)47.
[11] T. Tran, K. Kinoshita, J. Electroanal. Chem. 386(1995)221.
[12] V. Suryanarayanana, M. Noel, J. Power Sources 94(2001)137.
[13] W. Lu, D.D.L. Chung, Carbon 41(2003)945.
[14] Y. Ein-Eli, B. Markovsky, D. Aurbach, Y. Carmeli, H. Yamin, S. Luski, Electrochim. Acta 39(1994)2559.
[15] M.R. Wagner, J.H. Albering, K.-C. Moeller, J.O. Besenhard, M. Winter, Electrochem. Commun. 7(2005)947.
[16] W. Lu, D.D.L. Chung, Carbon 39(2001)493.
[17] J.-C. Panitz, U. Wietelmann, M. Wachtler, S. Ströbele, M. Wohlfahrt-Mehrens, J. Power Sources 153(2006)396.
[18] P. Novák, F. Joho, R. Imhof, J.-C. Panitz, O. Haas, J. Power Sources 81–82(1999)212.
[19] A.-K. Hjelm, G. Lindbergh, A. Lundqvist, J. Electroanal. Chem. 506(2001)82.
[20] J.S. Hong, J.R. Selman, J. Electrochem. Soc. 147(2000)3190.
[21] K. Dokko, M. Mohamedi, Y. Fujita, T. Itoh, M. Nishizawa, M. Umeda, I. Uchida, J. Electrochem. Soc. 148(2001)A422.
[22] K.S. Hwang, T.H. Yoon, C.W. Lee, Y.S. Son, J.K. Hwang, J. Power Sources 75(1998)13.
[23] M. Jean, C. Desnoyer, A. Tranchant, R. Messina, J. Electrochem. Soc. 142(1995)2122.
[24] N. Takami, A. Satoh, T. Ohsaki, M. Kanda, J. Electrochem. Soc.145(1998)478.
[25] P. Yu, B.N. Popov, J.A. Ritter, R.E. White, J. Electrochem. Soc. 146(1999)8.
[26] B. Markovsky, M.D. Levi, D. Aurbach, Electrochim. Acta 43(1998)2287.
[27] A. Funabiki, M. Inaba, Z. Ogumi, S.I. Yuasa, J. Otsuji, A. Tasaka, J. Electrochem. Soc. 145(1998)172.
[28] G. Sandi, R.E. Winans, K.A. Carrado, J. Electrochem. Soc. 143(1996)L95.
[29] T. Doi, K. Miyatake, Y. Iriyama, T. Abe, Z. Ogumi, Carbon 42(2004)3183.
[30] T. Doi, Y. Iriyama, T. Abe, Z. Ogumi, Electrochem. Commun. 7(2005)10.
[31] M.D. Levi, K. Gamolsky, D. Aurbach, U. Heider, R. Oesten, J. Electroanal. Chem.

477(1999)32.
[32] A.V. Churikov, M.A. Volgin, K.I. Pridatko, Electrochim. Acta 47(2002)2857.
[33] R.M. Wightman, D.O. Wipf, in: A.J. Bard (Ed.), Electroanalytical Chemistry, vol. 15, Marcel Dekker, New York, 1989.
[34] K. Aoki, J. Electroanal. Chem. 488 (2000)25.
[35] K. Aoki, A. Baars, A. Jaworski, J. Osteryoung, J. Electroanal Chem.472(1999)1.
[36] C. Capiglia, Y. Saito, H. Kageyama, P. Mustarelli, T. Iwamoto, T.Tabuchi, H. Tukamoto, J. Power Sources 81–82(1999)859.
[37] R. Vacassy, H. Hofmann, N. Papageorgiou, M. Grätzel, J. Power Sources 81–82(1999)621.
[38] J.S. Newman, Electrochemical Systems, Prentice-Hall Inc., Englewood Cliffs, 1973, p. 344.
[39] P.W. Atkins, Physical Chemistry, sixth ed., Oxford University Press, Oxford, 1998, p. 948.
[40] F. Tuinstra, J.L. Koenig, J. Chem. Phys. 53(1970)1126.
[41] G. Katagiri, Tanso 175(1996)304.
[42] F. Alloin, S. Bayoud, B. Azimipour, L. Reibel, J. Sanchez, Electrochim. Acta 45(2000)1193.
[43] Y. Hyung, D. Vissers, K. Amine, J. Power Sources 119–121(2003)383.
[44] I. Isaev, G. Salitra, A. Soffer, Y.S. Cohen, D. Aurbach, J. Fischer, J. Power Sources 119–121(2003)28.
[45] J. Vondrák, J. Reiter, J. Velická, B. Klápště, M. Sedlaříková, J. Dvořák, J. Power Sources 146 (2005)436

Chapter 3

Transition of current of lithium intercalation from solution to graphite

3.1 Introduction

Understanding of transfer mechanisms of lithium through a solution|graphite interface is useful for enhancement of current density and repeatability of secondary lithium batteries. Lithium ion in solution of the batteries is reduced electrochemically at the graphite surface to be transported into the graphite, called intercalation. In contrast, the intercalating lithium is oxidized at the interface to be released to the solution, called de-intercalation [1]. Rate-determining steps of the intercalation have been thought to be diffusion [2,3], electron transfer reaction rates [2,4] and trapping [5]. A measure of the transfer rate is the true and the apparent diffusion coefficients of lithium in graphite. In order to evaluate the diffusion coefficient, it is necessary to circumvent complications associated with ohmic resistance [6], interaction between intercalating lithium atoms [4,7], dependence of the diffusion coefficient on the concentration of lithium [2,8,9], validity of the Nernst equation [4,8,10], and time-scale of reaching the equilibrium [6]. However, reported values of the diffusion coefficient have ranged from 10^{-16} to 10^{-6} cm^2 s^{-1}, and hence are regarded as actually unknown.

The transport kinetics has been investigated by means of cyclic voltammetry [2,11,12], chronoamperometry [13,14], the potentiostatic and galvanostatic intermittent titration techniques [2,6,15–17], and electrochemical impedance spectroscopy [14,15,18–23]. The analysis of impedance data depends on so many varieties of electric circuit models that the transport data include necessarily much ambiguity. In contrast, the intermittent techniques can avoid the complication by carrying out the transition from such a quasi-equilibrium state that the complications may be minimized. The difficulty in analyzing the transport lies in determination of concentrations of intercalating Li, partly because of unavailable uniform distribution of the intercalated graphite and partly because of instability of intercalating lithium at the determination. Only the available technique is potentiometry on the assumption of the Nernst equation. If potentiometry includes 60 mV errors, the prediction of the current amounts to ten times difference, leading to hundred times errors for the diffusion coefficient.

Our suggestion here of acquiring reliable data is to use the conventionally known transport behavior of Li^+ in solution which is responsible for the transport of Li in graphite. An

increase in concentration of Li^+ in solution is expected to alter the rate-determining step of the transport in solution to that in graphite. Then the information of the transport in the solution may be reflected on that in the graphite. Our aim is to evaluate the diffusion coefficient of Lithium in graphite from that of Li^+ in solution. The solvent should be so simple that the Stokes–Einstein equation can be applied to the estimation of diffusion coefficient. The simplest solvent is acetonitrile rather than a mixture of ethylene carbonate (EC) and diethyl carbonate (DEC). We will carry out linear sweep voltammetry and chronoamperometry for the intercalation at various concentrations of Li^+, paying attention to the time-dependent variation of the mass transport. We also present the theory for chronoamperometry of which transport can take over both phases. The intercalation of Li^+ has often been conducted in a mixture of EC and DEC. Moisture included in the solvent has been removed by lithium metal which has also been used as a reference electrode, and then the dissolution of the metal has changed the concentration of Li^+. Since our aim is to control concentrations of Li^+ accurately, we will use here acetonitrile as a solvent, of which moisture can be removed by adding molecular sieves.

3.2 Experimental

Lithium perchlorate (Wako, Tokyo) was used as received. Acetonitrile (Wako, Tokyo) was treated with over-amount molecular sieves 4A1/8 (Wako, Tokyo) in order to remove moisture. Other chemicals used were of analytical grade. Solutions for voltammetry were bubbled with highly purified nitrogen before voltammetric run and kept in nitrogen atmosphere during experiments.

Cyclic voltammetry was performed with a computer-controlled Potentio/Galvanostat, Model 1112 (Huso, Kawasaki) at room temperature in a three-electrode cell. The working electrode was a pyrolytic graphite electrode (PGE) (BAS Inc, Tokyo) 3 mm in diameter. A platinum coil and a Ag|AgxO were used as the counter and the reference electrodes, respectively. The potential difference of a Ag|AgxO reference electrode from a Ag|AgCl was by -0.054 V lower than that at the Ag|AgCl. Before each measurement, the PGE was polished with 0.05 μm alumina slurry on a wetted cotton cloth and rinsed with acetonitrile in the ultrasonic bath for 1 min before each voltammetric run. The exposition of the crystallinity has been demonstrated previously by means of Raman spectra [24]. The Ag|AgxO reference electrode was made by immersing a mechanically polished silver wire into concentrated nitric acid until its surface turned to grey (normally in 10 min). The as-prepared electrode showed a drift of equilibrium potential within a

few millivolts.

3.3 Results

Fig 3-1 shows cyclic voltammograms of different concentrations of $LiClO_4$, c_1^*, at the PGE in acetonitrile after removing oxygen and moisture. Since the voltammograms are similar to those in dimethyl sulfoxide (DMSO), propylene carbonate (PC) and dimethyl formamide (DMF) [25], both the intercalation and the de-intercalation should occur also in acetonitrile. The cathodic wave at about -2.5 V for $c_1^* < 14$ mM has been assigned to the intercalation of Li^+ into the graphite, whereas the anodic one at -1.1 V has been assigned to the de-intercalation of Li from the PGE [24]. The reaction can be described as follows [26,27]: $Li+ + e^- + (1/z)\ C_6 \leftrightarrow (1/z)\ Li_zC_6$. Current values at c_1^* =10 and 50 mM had little difference in spite of five times difference in the concentration (solid and dashed curves in Fig 3-1), suggesting a minor contribution of diffusion of Li^+ or the first-order kinetics of Li^+ in the solution. In contrast, the cathodic current for 1.0 M Li^+ at -2.5 V was smaller than those for 10 and 50 mM, in accordance with the smaller anodic current at -1.1 V. The inhibition of the intercalation and de-intercalation at 1 M Li^+ is ascribed to high content of water from crystal of $LiClO_4$, as has been demonstrated in Fig 3-2 of the previous work [24].

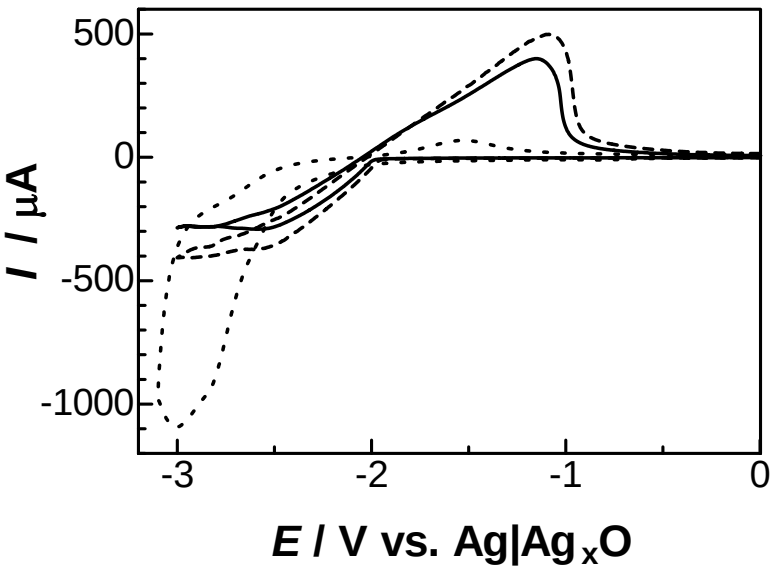

Fig 3-1. Cyclic voltammograms of 10 mM (solid line), 50 mM (dashed line) and 1.0 M (dotted line) $LiClO_4$ in dried acetonitrile without oxygen at the PGE for v = 50 mV s^{-1}.

Fig 3-2 shows the dependence of cathodic peak current, $I_{p,c}$, on c_1^* in acetonitrile. The current was proportional to c_1^* for $c_1^* < 10$ mM, whereas it kept a constant for $c_1^* > 15$ mM. A rate-determining step, related with the intercalation of Li^+, must change in the domain 10–15 mM. An evidence of the intercalation is the de-intercalating charge, Q_a, which should be equivalent to the intercalating charge [24]. The de-intercalating charge evaluated from the area of the anodic

wave at -1.1 V was plotted against c_1^* in Fig 3-2, showing the variation similar to the cathodic peak current. Therefore the cathodic current at -2.5 V ought to cause necessarily the intercalation, and hence the intercalation should be inhibited for $c_1^* > 15$ mM.

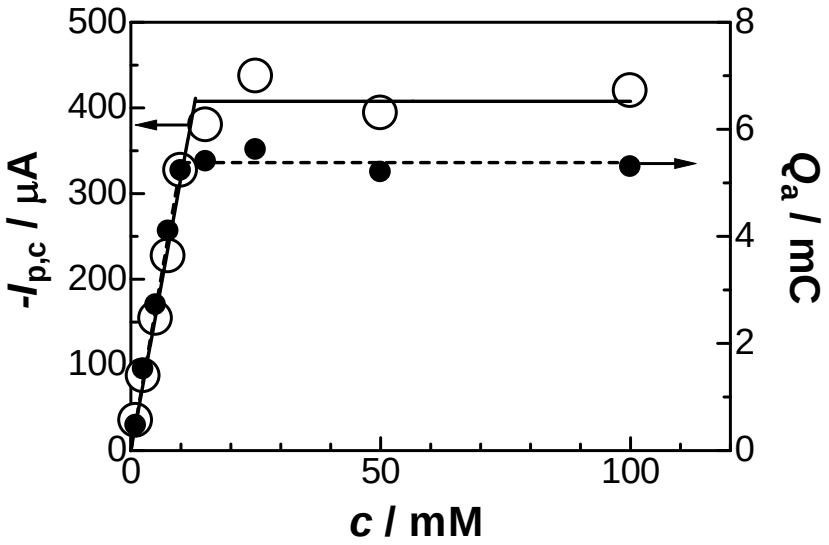

Fig 3-2. Variation of the cathodic peak current, $I_{p,c}$, (open circles) and the anodic charge, Q_a, (full circles) with the concentration, c_1^*, of $LiClO_4$ in deaerated and dried acetonitrile at $v = 50$ mV s^{-1}.

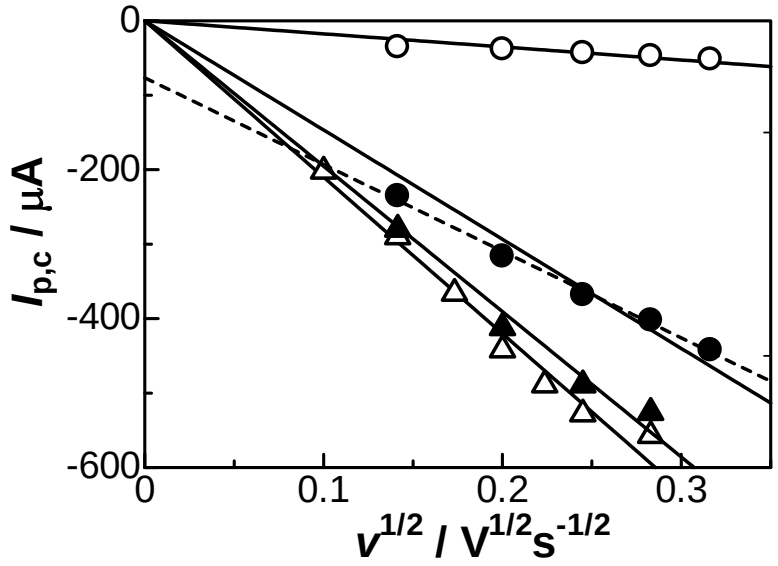

Fig 3-3. Dependence of the cathodic peak currents on the square-roots of scan rates for c_1^* = (a) 1, (b) 10, (c) 50 and (d) 100 mM from the top to the bottom. The dashed line is obtained by regression without forcing a line to pass through the origin.

We plotted values of the cathodic peak current against the square-root of the scan rates in Fig 3-3 for several concentrations. All variations were shown to be proportional, regardless of the concentrations. The proportionality indicates a diffusion or diffusion-like control of the intercalation although the rate-determining step for $c_1^* < 10$ mM was different from that for $c_1^* > 15$ mM. We have already concluded that the cathodic current for $c_1^* < 10$ mM was controlled by migration-diffusion of Li^+ in solution [24]. It is predicted that the current for $c_1^* > 15$ mM may also be controlled by diffusion of Li in the graphite, although it is well-known that electrochemical products (here Li) do not control mass transport

under conventional conditions. In order to distinguish diffusion of Li^+ in solution from diffusion of Li in the graphite, we examined effects of convection of the solution on the cathodic current. When the solution was stirred vigorously with a magnetic stirrer, the current of 5 mM Li^+ solution exhibited time fluctuation, as is shown in Fig 3-4. In contrast, no fluctuation appeared in the current of 50 mM Li^+ solution, indicating a rate-determining step either at the interface or in the graphite rather than in the solution. We do not know any surface process with the proportionality to $v^{1/2}$, to our knowledge. Thus it is reasonable to attribute the proportionality for c_1^* > 15 mM to diffusion of Li in the graphite. Solid films have been reportedly formed at -2.2 V vs. Ag|AgCl at an expense of decomposition of solvent [28,29]. Our multiple potential scan voltammograms showed only 10% decrease in the current at each cycle. Even if films are formed, they have minor effects on the current. We noticed a possibility of the decomposition of acetonitrile because the cathodic current was not totally dependent on the scan rate, as is demonstrated by the appearance of the intercept in the plot for 10 mM in Fig 3-3b. The more direct evidence is the insufficient compensation of the intercalation charge with the de-intercalation one (80%) [24].

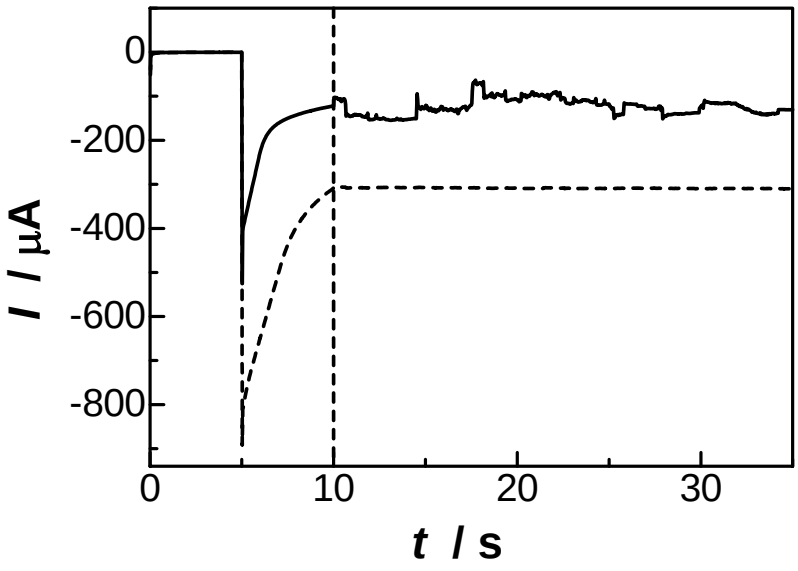

Fig 3-4. Chronoamperometric curves of 5 (solid curve) and 50 mM $LiClO_4$ (dashed curve) solution at the PGE after the potential was stepped from -0.5 to -2.7 V. The solution was stirred with a magnetic stirrer vigorously from 5 to 30 s at the potential - 2.7 V.

The diffusion flux of Li in graphite has been reported to vary complicatedly with concentrations of intercalating Li [8,9], with the intercalated structure in the form of Li_zC_6 for $0 < z < 1$ [2,8,10], with structural change in the intercalated graphite [30], and with phenomenological dependence of the diffusion coefficient on the concentration [31]. If the diffusion coefficient varies really with concentrations, the Cottrell equation in chronoamperometry should not hold. For example, a decrease in the diffusion coefficient with an increase in the concentration should provide a negative intercept at the Cottrell plot. Thus it is worth while to

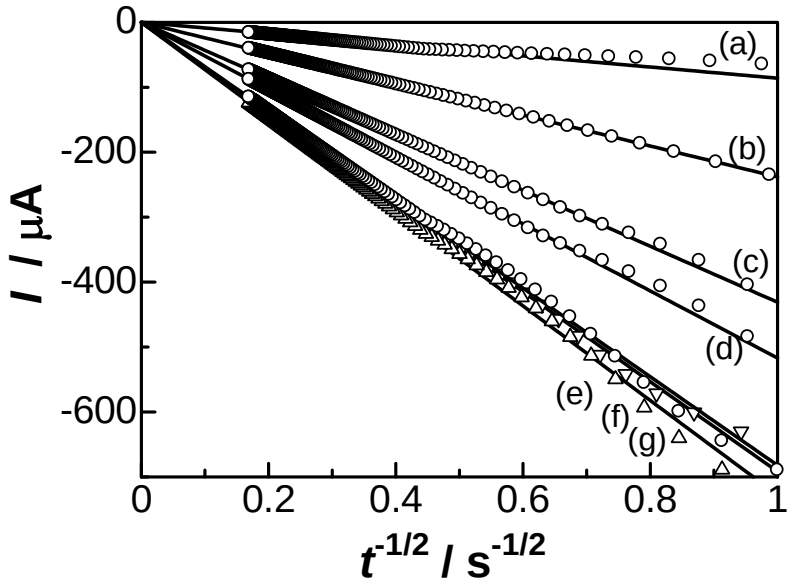

Fig 3-5. Cottrell plots for solutions with c_1^* = (a) 1 (b) 5, (c) 15, (d) 25, (e) 50, (f) 75, (g) 100 mM when the potential was stepped from -0.5 to -2.7 V.

examine the validity of the Cottrell equation. Chronoamperometry was made at -2.7 V in various concentrations of quiescent Li^+ solutions. The Cottrell plots for $1 \le c_1^* \le 100$ mM fell on each line with the zero intercept, as is shown in Fig 3-5. Therefore, the dependence of diffusion coefficient on the concentration can be neglected within the error of the Cottrell plots. The slope increased with an increase in the concentration until 50 mM. It kept a constant at concentrations over 50 mM. This variation was very close to that in Fig 3-2.

3.4 Theory of chronoamperometry

3.4.1 Nernst equation

Lithium ion in solution is reduced at a graphite electrode to intercalating lithium:

$Li^+(solution) + e^- \leftrightarrow Li(graphite)$ (1)

Its Nernst equation can be written in the formal way as

$E = E^o + (RT/F)\ln[a(Li^+)/a(Li)]$ (2)

where a(X) is the activity of species X. Diffusion of Li in the graphite is much slower than that of Li^+ in the solution. When Li^+ is reduced at a steady potential close to the domain of the limiting current, a value of $a(Li^+)/a(Li)$ in Eq.(2) become very small, keeping constant. A value of $a(Li^+)$ or concentration of Li^+ increases gradually by diffusion through the solution (see Fig 3-6). Correspondingly a value of a(Li) or concentration of Li at the interface increases, and Li should be accumulated in the vicinity of the interfacial domain on the graphite side. However, the concentration is limited by the maximum of Li in the graphite of the form, LiC_6. Once the concentration reaches the maximum, the constancy of $a(Li^+)/a(Li)$ can be maintained only by

keeping the surface concentration of Li^+ a value less than c_1^* (see from the dashed to the solid curve in Fig 3-6). Then diffusion in the solution phase is controlled by that in the graphite. Generally speaking, mass transport of a reactant is controlled by that of a product. This is unusual electrochemical behavior, and hence it is necessary to consider a Nernst equation in which values of a(Li) have a maximum.

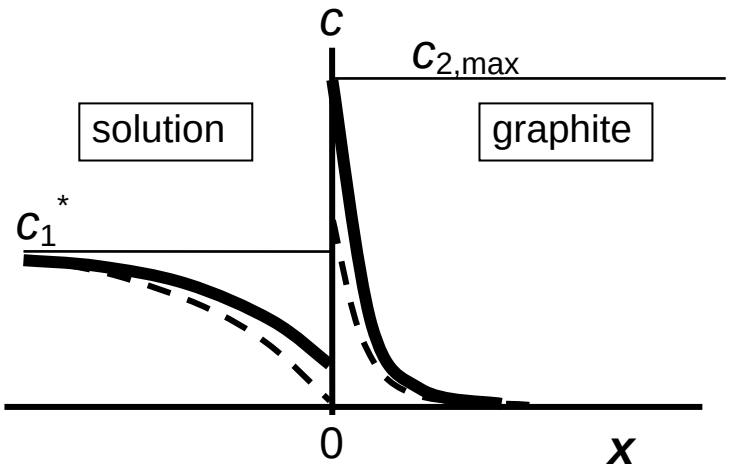

Fig 3-6. Illustration of concentration profiles in the solution phase ($x < 0$) and the graphite one ($x > 0$) at a short (dashed curve) and a long (solid curve) electrolysis.

We apply the Langmuir adsorption model to the maximum occupation of Li in graphite in order to represent the saturation of Li in graphite. Prosine et al have used Frumkin-type isotherm for the limitation of the intercalation to $LiFePO_4$ [10]. According to a textbook of statistical mechanics [32], the inverse coverage of an adsorbed species is given by

$$1/\theta = 1 + \exp\left(-(\varepsilon_0 + \mu)/RT\right) \quad (3)$$

where ε_0 is the adsorption energy of Li on the PGE and μ is the chemical potential of Li in the PGE. By solving Eq. (3) with respect to μ, the electrochemical potential of Li is written as

$$\overline{\mu}_{\mathrm{Li}} = -\varepsilon_0 + RT\ln[\theta/(1-\theta)] \quad (4)$$

The electrochemical potentials of Li^+ and the electron are expressed by, respectively

$$\overline{\mu}_{\mathrm{Li+}} = \mu^{\mathrm{o}}_{\mathrm{Li+}} + RT\ln a_{\mathrm{Li+}} + F\phi_{\mathrm{s}} \quad (5)$$

$$\overline{\mu}_{\mathrm{e}} = \mu^{\mathrm{o}}_{\mathrm{e}} - F\phi_{\mathrm{E}} \quad (6)$$

Here ϕ_{s} and ϕ_{E} are inner potentials in the solution phase and the electrode (graphite) phase, respectively. Inserting Eqs. (4)-(6) into the equilibrium condition, $\overline{\mu}_{\mathrm{Li+}} + \overline{\mu}_{\mathrm{e}} = \overline{\mu}_{\mathrm{Li}}$ yields

$$E = E^{\mathrm{o}} + (RT/F)\ln[a_{\mathrm{Li+}}(1-\theta)/\theta] \quad (7)$$

where E is the electrode potential defined by $(\phi_{\mathrm{E}} - \phi_{\mathrm{s}})/F$, and E^{o} is the standard potential given by $(\mu^{\mathrm{o}}_{\mathrm{Li+}} + \mu^{\mathrm{o}}_{\mathrm{e}} + \varepsilon_0)/F$. Expressing the maximum concentration and any concentration of Li in graphite as $c_{2,\max}$ and c_2, respectively, and rewriting $a_{\mathrm{Li+}}$ by c_1/c^{o}, Eq.(7) becomes

$$E = E^{\mathrm{o}} + (RT/F)\ln[c_1(c_{2,\max} - c_2)/c^{\circ}c_2] \quad (8)$$

where c^o is the standard concentration (1 M). This is the Nernst equation modified for the saturation of Li in graphite, and holds at the interface between the solution and the PGE. It will be applied to the mass transport problems by chronoamperometry as the boundary condition at the interface.

3.4.2 Mass transport of Li^+ in solution

We take the x-axis normal to the planar surface of the PGE, assigning $x > 0$ to the PGE phase and $x < 0$ to the solution phase, as is illustrated in Fig 3-6. The mass transport of Li^+ and an anion in the solution phase is controlled by Nernst-Planck equations because the solution has no supporting electrolyte. The Nernst-Planck equations for Li^+, denoted 1, and A (anion or counterion) at $x < 0$ are given by respectively

$$J_1 = -D_1 \partial c_1 / \partial x - (F/RT) D_1 c_1 \partial \phi / \partial x \quad (9)$$

$$J_A = -D_1 \partial c_A / \partial x + (F/RT) D_1 c_A \partial \phi / \partial x \quad (10)$$

where ϕ is the inner potential at x, J is the flux, and c is the concentration. Here we have assumed that the diffusion coefficients of Li^+ and the anion have a common value, D_1. Combining these equation with the equation of continuum, $\partial c / \partial t = -D(\partial J / \partial x)$, we have

$$\partial c_1 / \partial t = D_1 \partial^2 c_1 / \partial x^2 + (D_1 F / RT) \partial (c_1 \partial \phi / \partial x) / \partial x \quad (11)$$

$$\partial c_A / \partial t = D_1 \partial^2 c_A / \partial x^2 - (D_1 F / RT) \partial (c_A \partial \phi / \partial x) / \partial x \quad (12)$$

The summation of Eqs. (11) and (12) on the electric neutrality condition, $c_1 = c_A$, yields

$$\partial c_1 / \partial t = D_1 \partial^2 c_1 / \partial x^2 \quad (13)$$

The subtraction of Eq.(11) from Eq.(12) yields

$$\partial (c_1 \partial \phi / \partial x) / \partial x = 0 \quad \text{or} \quad c_1 \partial \phi / \partial x = B_3 \quad (14)$$

where B_3 is a constant.

The initial conditions before the potential application are $c_1 = c_1^*$ and $c_A = c_1^*$. The boundary conditions are

$$x \to -\infty : c_1 \to c_1^* \quad \text{and} \quad c_A \to c_1^* \quad (15)$$

The Laplace transform of Eq.(13) with the initial condition is

$$s\overline{c_1} - c_1^* = D_1 \mathrm{d}^2 \overline{c_1} / \mathrm{d}x^2$$

of which solution with the condition (15) is given by

$$\overline{c_1} = c_1^* / s - B_1 \exp\left(\sqrt{s / D_1}\, x\right) \quad (16)$$

Similarly, the solution for species A is give by

$$\overline{c}_A = c_1^* / s - B_1 \exp\left(\sqrt{s / D_1}\, x\right) \quad (17)$$

The flux for Li^+ yields the current density, j (= FJ), whereas there is no flux for the anoin. Applying these relations to Eqs. (9) and (10), we obtain at $x = 0$

$$j/F = -D_1\left(\partial c_1/\partial x\right)_{x=0} - (D_1F/RT)\left(c_1\partial\phi/\partial x\right)_{x=0} \quad (18)$$

$$0 = -D_1\left(\partial c_A/\partial x\right)_{x=0} + (D_1F/RT)\left(c_A\partial\phi/\partial x\right)_{x=0} \quad (19)$$

Inserting Eqs. (14), (16) and (17) into the Laplace transformed Eqs. (18) and (19), we have

$$\bar{j}/F = B_1\sqrt{D_1 s} - (D_1F/RT)B_3 \quad (20)$$

$$0 = B_1\sqrt{D_1 s} + (D_1F/RT)B_3 \quad (21)$$

The sum of Eqs. (20) and (21) yields

$$\bar{j}/F = 2B_1\sqrt{D_1 s} \quad (22)$$

Eliminating B_1 from Eqs. (16) and (22), we obtain at $x = 0$

$$\left(\overline{c_1}\right)_{x=0} = c_1^*/s - \bar{j}/2F\sqrt{D_1 s} \quad (23)$$

The inverse Laplace transformation of Eq.(23) becomes

$$\left(c_1\right)_{x=0} = c_1^* - \frac{1}{2F\sqrt{\pi D_1}}\int_0^t \frac{j(u)\mathrm{d}u}{\sqrt{t-u}} \quad (24)$$

This is the relation of the concentration of Li^+ at the interface with the time-dependent current density.

3.4.3 Mass transport of Li in graphite phase

The mass transport of Li in the graphite phase ($x > 0$) is controlled only by diffusion, of which equation is given by

$$\partial c_2/\partial t = D_2\left(\partial^2 c_2/\partial x^2\right) \quad (25)$$

where D_2 is the diffusion coefficient of Li in the graphite phase. The Laplace transformed solution of Eq.(25) satisfied with $c_2 = 0$ for $t = 0$ and $x \to \infty$ is given by

$$\overline{c_2} = B_2\exp\left(-\sqrt{s/D_2}\,x\right) \quad (26)$$

The flux at $x = 0$ should not be accumulated (no adsorption), and hence the current density is expressed by $j/F = -D_2\left(\partial c_2/\partial x\right)_{x=0}$. Inserting Eq.(26) into this equation and taking the Laplace transformation, we obtain

$$\bar{j}/F = B_2\sqrt{D_2 s} \quad (27)$$

Eliminating B_2 from Eqs.(26) and (27), setting x to be 0, and carrying out the inverse Laplace transformation, we have

$$\left(c_2\right)_{x=0} = \frac{1}{F\sqrt{\pi D_2}}\int_0^t \frac{j(u)\mathrm{d}u}{\sqrt{t-u}} \quad (28)$$

This expresses the relation between the concentration of Li at the interface and the time-dependent current density.

3.4.4 Combination of mass transport and Nernst equation

Reaction (1) holds at the interface ($x = 0$). Taking x to be 0 in Eq.(8), we have

$$e^{\varsigma} = (c_1)_{x=0}\{c_{2,\max} - (c_2)_{x=0}\} / c_1^*(c_2)_{x=0} \quad (29)$$

where

$$\varsigma = F(E - E^{\circ}) / RT - \ln(c_1^* / c^{\circ}) \quad (30)$$

Inserting Eqs. (24) and (28) into Eq.(29), we have

$$f^2 - \{X(1 + e^{\varsigma}) + Y\} f + XY = 0 \quad (31)$$

where $X = 2c_1^* \sqrt{D_1}$, $Y = c_{2,\max} \sqrt{D_2}$ and

$$f = \frac{1}{F\sqrt{\pi}} \int_0^t \frac{j(u)\mathrm{d}u}{\sqrt{t-u}} \quad (32)$$

A solution of the quadratic equation for f in Eq.(31) is

$$f = \left[X(1 + e^{\varsigma}) + Y \pm \sqrt{\{X(1 + e^{\varsigma}) + Y\}^2 - 4XY} \right] / 2 \quad (33)$$

The plus positive sign in Eq.(33) makes a value of $c_{2,\max}$- c_2^* in the Nernst equation negative. Thus the negative sign is used. Since X, Y and e^{ζ} are independent of the time, the solution of the integral equation (32) is

$$j = \frac{FY}{2\sqrt{\pi t}} \left[p(1 + e^{\varsigma}) + 1 - \sqrt{\{p(1 + e^{\varsigma}) + 1\}^2 - 4p} \right] \quad (34)$$

where

$$p = X / Y = 2c_1^* \sqrt{D_1} / c_{2,\max} \sqrt{D_2} \quad (35)$$

For $\zeta \rightarrow -\infty$, Eq.(35) is reduced to

$$j = \frac{FY}{2\sqrt{\pi t}} [p + 1 - |p - 1|]$$

which leads for $0 < p < 1$ to

$$j = FYp / \sqrt{\pi t} = Fc_{2,\max} \sqrt{D_2} / \sqrt{\pi t} \quad (36)$$

and for $p > 1$ to

$$j = FX / \sqrt{\pi t} = 2Fc_1^* \sqrt{D_1} / \sqrt{\pi t} \quad (37)$$

Values of the terms in the bracket in Eq. (34) ($2\sqrt{\pi t}\, j / Fc_{2,\max}\sqrt{D_2}$, the dimensionless current density) are shown for some values of ζ in Fig 3-7. The current for $p < 1$ is controlled by the mass transport of Li^+ in the solution due to both electric migration and diffusion. In contrast, the current for $p > 1$ is controlled by diffusion of Li in the graphite phase. The two rate-determining steps vary sharply at $p = 1$ in the limiting current domain ($E < E^o$). The sharp variation indicates either mass transport control in the solution or in the graphite, without any mixed control. Therefore, $p = 1$ is a critical point at which

$$2c_1^* \sqrt{D_1} = c_{2,\max}\sqrt{D_2} \qquad (38)$$

holds. The factor 2 is ascribed to the electric migration [33,34].

3.5 Discussion

According to Eq. (36), the chronoamperometric current at low concentrations is proportional to $t^{-1/2}$. From the slope, we evaluated D_1 to be 1.53×10^{-5} cm^2 s^{-1} in acetonitrile. Applying the Stokes–Einstein equation [35] to this value of D_1, we estimated the diameter of Li^+ in acetonitrile to be 0.83 nm for the viscosity of acetonitrile, 0.341 MPa s. In contrast, the diameters of Li are reported to be 0.29 nm by the atomic model, 0.27 nm by the covalent bond and 0.36 nm by the Van del Waals model. The larger diameter evaluated from the diffusion coefficient is obviously due to the solvation effect.

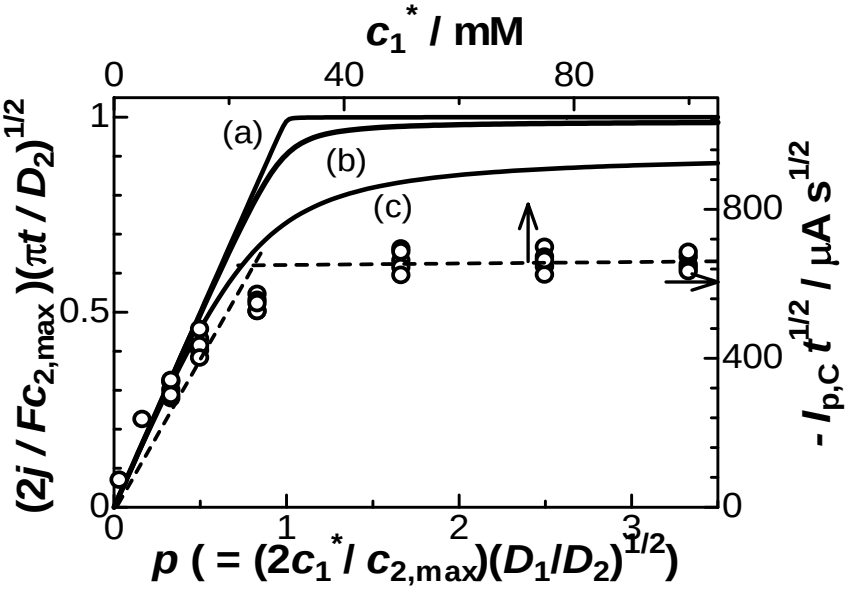

Fig 3-7. Variation of the dimensionless chronoamperometric current with p for $E - E^o$ = (a) -0.237, (b) -0.118, and (c) -0.059 V, calculated from Eq.(34) at 25°C. The points are the slopes of the Cottrell plots for various concentrations of Li^+ in the right axis and the upper axis.

Since a variable involved in p is only c_1^*, the theoretical curves in Fig 3-7 should be equivalent to the plot of the slope of the Cottrell plot against c_1^*. Fig 3-7 shows the experimental results. The

variation is close to the theoretical one although there was no sharp critical change in the slope. The chronoamperometric current was so large that the *IR*-drop of the solution resistance did not satisfy the limiting current conditions [24]. Actually, the experimental plot is close to curve (c) for $E - E_o$ = -0.059 mV or $(c_1)_{x=0} = 0.1c_1^*$.

It is predicted that deliberately continuous variation of c_1^* at a steady-state current may yield a sharp variation of the current, because the steady-state current is so smaller than the transient current that the *IR*-drop has negligible contribution. As a technique of varying continuously the concentration, we added concentrated $LiClO_4$ solution at a given speed by use of a titration tube to the acetonitrile solution which was stirred with a magnetic stirrer. Then we got the current vs. time or vs. concentration curve, as is shown in Fig 3-8. The current for c_1^* < 10 mM was fluctuated owing to the fluctuated convection, and the averaged absolute values increased with the concentration. The absolute values of the currents decreased at c_1^* = 10 mM, although c_1^* was increased. The decrease is caused by the restriction of the mass transfer of Li owing to $D_2 << D_1$, and is roughly obeyed by the Cottrell equation.

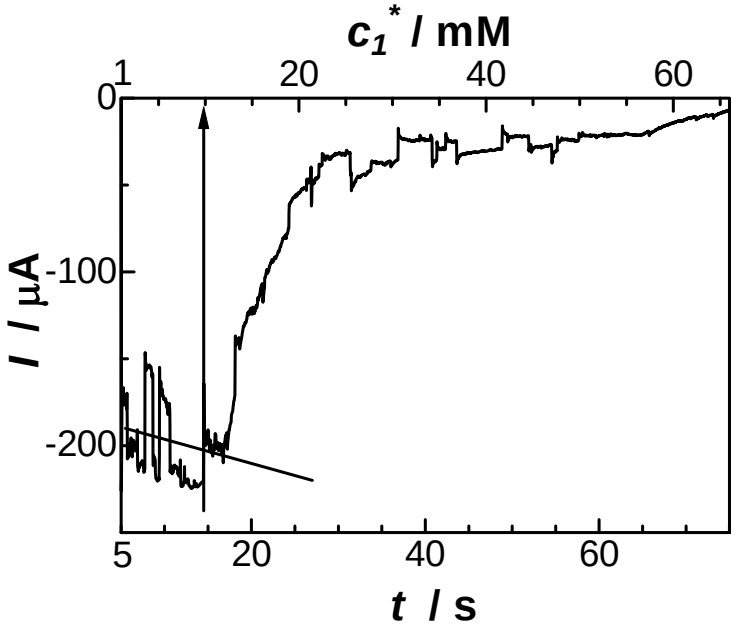

Fig 3-8. Concentration-variation of the current at the PGE for -2.7 V in the $LiClO_4$ solution which was stirred with a magnetic stirrer. The concentration was varied by titrating 0.5 M $LiClO_4$ solution into 1.0 mM $LiClO_4$ solution at the rate of 2.57 cm^3 min^{-1}.

According to the variations of the current with the concentration, c_1^* = 10 mM can be regarded as the critical concentration. From Eq.(38) at the critical concentration, the value on the left hand side is known. If $c_{2,max}$ is the concentration in the form of LiC_6, keeping the density of graphite, 2 g cm^{-3}, it is given by

$$c_{2,max} = (2\ \mathrm{g\ cm^{-3}})/(12\ \mathrm{g\ mol^{-1}})/6 = 27.8\ \mathrm{M}$$

Then we can evaluate $D_2 = [2(c_1^*)_{cr}/c_{2,max}]^2 D_1 = 0.79\times10^{-11}$ cm^2 s^{-1}. This value is close to

0.92×10^{-11} cm^2 s^{-1} by simulation to voltammograms [17,31]. However, a number of larger values were reported: 10^{-5}-$10^{-9}$$cm^2$ s^{-1}depending on the electrode potential by the ac impedance[19], 5×10^{-11} cm^2 s^{-1} for curve fitting of voltammograms [30], over 1.25×10^{-9} cm^2 s^{-1} [7] and 4.6×10^{-8} cm^2 s^{-1} [36] by galvanostatic technique, 2.0-4.7×10^{-10} cm^2 s^{-1} by slow cyclic voltammetry [2], 1.0×10^{-10} cm^2 s^{-1} for simulation to voltammograms [12], chronoamperometry [37] and the charge ratio [38], and 2.0×10^{-11} - 2.0×10^{-9} cm^2 s^{-1} by galvanostatic and potentiostatic intermittent titration [39]. On the other hand, smaller values, 0.4-7×10^{-16} cm^2 s^{-1} by galvanostatic and potentiostatic intermittent titration on the phase field model [16] and 4.4-13×10^{-12} cm^2 s^{-1} in HF-cointercalated electrodes by impedance [40] were also reported. The wide scattering of the values may be ascribed mainly to ambiguity of realizing and evaluating uniform concentration of Li in graphite, and subordinately to insufficient potential control owing to *IR*-drop [6], variation of the reactions with electrode potentials [17,31,41] and with concentration [7,9,10], contributions of capacitance [36], and some kinetics of trapping [42], nucleation [39] and charge transfer rates [6,12].

We have assumed a common value of diffusion coefficients for Li^+ and anion in solution. Reported values of the diffusion coefficients of Li^+ and ClO_4^- in acetonitrile are 1.5×10^{-5} and 4.3×10^{-5} cm^2 s^{-1}. The maximum contribution of the difference in the diffusion coefficients to the diffusion-controlled current is known to be the square-root of the ratio of the two coefficients. The theoretical current may be at most 1.7 times larger than that under the assumption of the equi-value of the diffusion coefficients. Then the ordinate in Fig 3-7 varies by 1.7 times whereas the abscissa has no change. Here we just want to compare the experimental values on the abscissa with the theoretical ones on the abscissa. Consequently, the difference in diffusion coefficients has no effect on determining the critical concentration.

3.6 Conclusion

Cathodic voltammetric currents and chronoamperometric currents for the intercalation of Li^+ showed the diffusion-controlled like behavior, regardless of values of c_1^*. They were proportional to the concentrations for $c_1^* < 10$ mM, and hence were controlled by electric migration and diffusion. The diffusion coefficient of Li^+ in acetonitrile had a reasonable value (1.53×10^{-5} cm^2 s^{-1}). In contrast, the currents for $c_1^* > 15$ mM were independent of the concentrations without any effect of convection of the solution. These and the time-dependence with a diffusion type are an evidence of diffusion of Li inside of the graphite. We have confirmed that the current was due to the intercalation by equivalence of the intercalating charge and

de-intercalating one. Since the Cottrell plots for $c_1^* \leq 100$ mM always have passed through the origin, the diffusion coefficient can be regarded as independent of the concentrations as well as values of z of Li_zC_6. The value of the diffusion coefficient (0.79×10^{-11} cm^2 s^{-1}) indicates values of the thickness of the diffusion layer ($(\pi Dt)^{1/2}$) are 0.158 μm for 10 s electrolysis, 0.50 μm for 100 s, 3.0 μm for 1 h, 14.7 μm for 1 day, and 80 μm for 1 month. It is quite pessimistic to realize uniform distribution of intercalating Li in the thinnest commercially available graphite sheet (0.25 mm thin). In other words, the Li-intercalated graphite obtained by long-term electrolysis has not yet reached the equilibrium although it looks like under a steady-state. Therefore the determination of z by potentiometry includes large errors.

We will apply our data of the diffusion model to commercialized Li-ion batteries for portable devices of which the particle size ranges from 10 to 20 micrometer. The thickness of the diffusion layer at cathodic electrolysis for the time t is given by $(\pi Dt)^{1/2}$. Substituting the value of D (0.79×10^{-11} cm^2 s^{-1}) and 2 h for the electrolysis, we obtain $(\pi Dt)^{1/2}$ = 4.2 μm. The graphite is anodically charged within this diffusion layer. The percentages of the uncharged volume of graphite particles at 10 and 20 μm in diameter are $[(10-4.2\times2)/10]^3 = 0.004$ and $[(20-4.2\times2)/20]^3 = 0.19$. These values demonstrate almost full electrolysis in practical batteries.

We have derived conclusive expressions of Eqs.(36) and (37) for chronoamperometric currents and Eq.(38) for the condition of the critical concentration. They are based on the assumptions of the Langmuir isotherm and the equilibrium at the interface. We have no evidence to confirm the validity of this isotherm. However, the term, $1-\theta$, in Eq.(4) is responsible for the quadratic form of f in Eq.(31), which is a key of exhibiting the critical concentration. Therefore, the term, $1-\theta$, representing the limited vacancy in the graphite, is significant for the intercalation. The other assumption of the equilibrium is not practical but is useful for understanding concisely the significance of the term $1-\theta$. The latter assumption will be solved in future work.

3.7 References

[1] J.R. Dahn, R. Fong, M.J. Spoon, Phys. Rev. B 42(1990)6424.

[2] M.D. Levi, D. Aurbach, J. Electroanal. Chem. 421(1997)79.

[3] H.C. Shin, S.I. Pyun, S.W. Kim, M.H. Lee, Electrochim. Acta 46(2001)897.

[4] M.W. Verbrugge, B.J. Koch, J. Electrochem. Soc. 146(1999)833.

[5] J. Bisquert, Electrochim. Acta 47(2002)2435.

[6] M.D. Levi, E. Markevich, D. Aurbach, J. Phys. Chem. B 109(2005)7420.

[7] V.R. Subramanian, P. Yu, B.N. Popov, R.E. White, J. Power Sources 96(2001)396.
[8] M. Danielewski, W. Kucza, Solid State Ionics 172(2004)13.
[9] F. Lantelme, H. Groult, N. Kumagai, Electrochem. Acta 45(2000)3171.
[10] P.P. Prosini, M. Lisi, D. Zane, M. Pasquali, Solid State Ionics 148(2002) 45.
[11] J. Shim, K.A. Striebel, J. Power Sources 130(2004)247.
[12] M.W. Verbrugge, B.J. Koch, J. Electrochem. Soc. 143(1996)600.
[13] T. Uchida, Y. Morikawa, H. Ikuta, M. Wakihara, K. Suzuki, J. Electrochem. Soc. 143(1996)2606.
[14] Y. Nuli, J. Yang, Z. Jiang, J. Phys. Chem. Solids 67(2006)882.
[15] P. Yu, B.N. Popov, J.A. Ritter, R.E. White, J. Electrochem. Soc. 146(1999)8.
[16] B.C. Han, A. Van der Ven, D. Morgan, G. Ceder, Electrochim. Acta 49(2004)4691.
[17] M.D. Levi, E. Markevich, D. Aurbach, Electrochim. Acta 51(2005)98.
[18] N. Takami, A. Satoh, M. Hara, T. Ohsaki, J. Electrochem. Soc. 142(1995)371.
[19] A. Funabiki, M. Inaba, Z. Ogumi, S.I. Yuasa, J. Otsuji, A. Tasaka, J. Electrochem. Soc. 145(1998)172.
[20] T. Piao, S.M. Park, C.H. Doh, S.I. Moon, J. Electrochem. Soc. 146(1999)2794.
[21] Y.C. Chang, H.J. Sohn, J. Electrochem. Soc. 147(2000)50.
[22] M. Umeda, K. Dokko, Y. Fujita, M. Mohamedi, I. Uchida, J.R. Selman, Electrochim. Acta 47(2001)885.
[23] C. Ho, I.D. Raistrick, R.A. Huggins, J. Electrochem. Soc. 127(1980)343.
[24] X. Wang, K. Aoki, J. Electroanal. Chem. 588(2006)106.
[25] R. Santhanam, M. Noel, J. Power Sources 66(1997)47.
[26] S.B. Fagan, S. Guerini, J.M. Filho, V. Lemos, Microelectron. J. 36(2005)499.
[27] Y. Imai, A. Watanabe, J. Alloys Compd. in press, doi:10.1016/j.jallcom.2006.08.061
[28] M. Inaba, Z. Siroma, A. Funabiki, Z. Ogumi, Langmuir 12(1996)1535.
[29] A.C. Chu, J.Y. Josefowicz, G.C. Farrington, J. Electrochem. Soc. 144(1997)4161.
[30] S.I. Lee, Y.S. Kim, H.S. Chun, Electrochim. Acta 47(2002)1055.
[31] F. Lantelme, A. Mantoux, H. Groult, D. Lincot, Solid State Ionics 177(2006)205.
[32] R. Kubo, Statistical Mechanics, North-Holland, Amsterdam, 1965, p.243.
[33] K.B. Oldham, J. Electroanal. Chem. 337(1992)91.
[34] K. Aoki, A. Baars, A. Jaworski, J. Osteryoung, J. Electroanal. Chem. 472(1999)1.
[35] P.W. Atkins, Physical Chemistry, sixth ed., Oxford University Press, Oxford, 1998, p.749.

[36] A.A. Andriiko, P.V. Rudenok, L.I. Nyrkova, J. Power Sources 72(1998)146.

[37] A.M. Skundin, O.Yu. Grigor'eva, T.L. Kulova, S.V. Pouchko, J. Solid State Electrochem. 8(2003)11.

[38] X.C. Tang, C.Y. Pan, L.P. He, L.Q. Li, Z.Z. Chen, Electrochim. Acta 49(2004)3113.

[39] M.D. Levi, D. Aurbach, J. Phys. Chem. B 101(1997)4641.

[40] T. Nakajima, V. Gupta, Y. Ohzawa, H. Groult, Z. Mazej, B. Z˘ emva, J. Power Sources 137(2004)80.

[41] E. Deiss, Electrochim. Acta 47(2002)4027.

[42] J. Bisquert, V.S. Vikhrenko, Electrochim. Acta 47(2002)3977.

Chapter 4

Summary

The kinetic process of lithium intercalation on graphite electrodes consisted of the charge transfer of Li^+ from solution to the graphite surface, the reduction of Li^+ on the interface and the mass transfer of reduced Li from interface to the solid graphite was explored and interpreted through the conventional electrochemical methods.

The charge transfer of Li^+ ion on graphite electrode in acetonitrile was investigated in chapter 2**.** The rate-determining steps and redox potentials at zero current were interpreted on the basis of the voltammetric concept. The cathodic wave at concentrations less than 10 mM was controlled by diffusion and migration of Li^+ in the solution, whereas that at higher concentrations was by the intercalation kinetics. The anodic wave was caused by the de-intercalation, and behaved like an adsorption wave. The cathodic charge of the intercalation was larger by 30% than the anodic one because of side reaction of acetonitrile or impurities. The anodic and the cathodic peak potentials extrapolated to zero current were, respectively, -1.58 and -2.11 V vs. Ag|AgCl, which can be regarded as universal values. The difference in the peak potentials of intercalation and de-intercalation is 0.53 V, equivalent to 51 KJ mol^{-1}. This energy is an interfacial kinetic contribution of the intercalation and/or de-intercalation, and hence is lost at a cycle of the charge/discharge.

The mass transfer of reduced Li inside the solid graphite after intercalation showed interesting behavior in chapter 3. Intercalation current of Li^+ to a graphite electrode varied sharply with $[Li^+]$ from the proportionality to a constant, exhibiting critical behavior at $[Li^+]$ =10 mM. The cathodic peak current caused by the intercalation, was proportional to the square-root of the scan rate, irrespective of the concentrations. The current for $[Li^+] < 10$ mM is controlled both by diffusion and electric migration of Li^+ in solution, whereas that for $[Li^+] > 10$ mM is controlled by diffusion of Li in the graphite. The critical behavior was validated by the time-dependent mass transport theory, which was developed by use of the Nernst-Planck equation for the solution phase and the diffusion equation for the graphite one. Both equations were combined at the interface through a kind of the Nernst equation which contained a maximum concentration of Li in the graphite predicted from the structure of LiC_6. From the critical concentration, the diffusion coefficient of Li in the graphite was estimated to be 0.79×10^{-11} cm^2 s^{-1}, independent of the concentrations.

Acknowledgements

I would like to express my sincere appreciation to my supervisor, Professor Dr. Koichi Aoki (Department of Applied Physics & Fiber Amenity Engineering, University of Fukui) for his constant guidance, precious suggestion and invaluable contribution of time and intellect to prepare and submit this thesis.

I am very much thankful to Associate Professor Dr. Jingyuan Chen (Department of Applied Physics & Fiber Amenity Engineering, University of Fukui) for her helpful comments and encouragement.

I also thank Dr. Toyohiko Nishiumi and the group members who help me with this work.

I want to give my special thanks to my beloved husband, Dr. Nianjun Yang, and my family for their patience and help toward accomplishing this thesis.

I thank the Japanese friend Mr. Shouji Yoshida and his family for their help of my study, language and the daily life during the three years.

Sincerely yours

Xiaoxia Wang
Department of Applied Physics &
Department of Fiber Amenity Engineering
Graduate School of Engineering
University of Fukui